



# RETRACTED: Use of Ore-Derived Humic Acids With Diverse Chemistries to Elucidate Structure-Activity Relationships (SAR) of Humic Acids in Plant Phenotypic Expression

Richard T. Lamar<sup>1\*</sup>, Hiarhi Monda<sup>1</sup> and Rachel Sleighter<sup>2</sup>

<sup>1</sup> Bio Huma Netics, Inc., Gilbert, AZ, United States, <sup>2</sup> FBSciences, Inc., R&D, Norfolk, VA, United States

## OPEN ACCESS

### Edited by:

Spyridon Alexandros Petropoulos,  
University of Thessaly, Greece

### Reviewed by:

Luciano Pasqualoto Canellas,  
State University of the North  
Fluminense Darcy Ribeiro, Brazil  
Marta Fuentes,  
University of Navarra, Spain

### \*Correspondence:

Richard T. Lamar  
rich@bhni.us

### Specialty section:

This article was submitted to  
Plant Physiology,  
a section of the journal  
Frontiers in Plant Science

**Received:** 13 August 2021

**Accepted:** 20 October 2021

**Published:** 01 December 2021

### Citation:

Lamar RT, Monda H and  
Sleighter R (2021) Use  
of Ore-Derived Humic Acids With  
Diverse Chemistries to Elucidate  
Structure-Activity Relationships (SAR)  
of Humic Acids in Plant Phenotypic  
Expression.  
*Front. Plant Sci.* 12:758424.  
doi: 10.3389/fpls.2021.758424

We report the results of a structure-activity relationship study that was undertaken to identify humic substance chemistries that drive the plant biostimulant response. The effects of seven extensively chemically characterized, ore-derived humic acids (HA) on corn seedling biomass and root and shoot morphological parameters were investigated. Chemometric analyses were then conducted to identify correlations between HA chemical features and plant biomass and morphological characteristics. The primary chemical driver of plant biomass and morphology was the ratio between HA electron accepting capacity (EAC) and electron donating capacity (EDC). The HA electron accepting capacity is found in quinones and semiquinone free radicals, while the HA electron donating capacity is found in polyphenolics and glycosylated polyphenolics. Based on our results, we propose a mechanism of action for ore-derived HA plant biostimulation that involves the interplay of pro-oxidants, in the form of quinones and semiquinone radicals, and antioxidants, in the form of polyphenols and possibly glycones and carbohydrates. The quinones/semiquinones initiate an oxidative stress response via the stimulation of transmembrane electron flow that results in both reactive oxygen species (ROS) production (i.e., an oxidative burst) and membrane depolarization, the latter of which allows Ca<sup>2+</sup> flux from the apoplast into the cytoplasm. Based on the magnitude of depolarization, a specific cytoplasmic Ca<sup>2+</sup> signature is produced. As a secondary messenger Ca<sup>2+</sup>, via binding to Ca<sup>2+</sup>– sensor proteins, transmits the signature signal, resulting in specific intracellular responses that include changes to plant morphology. The greater the EAC, the greater the ROS production and magnitude of plasma membrane depolarization and resulting stress response. The HA antioxidants are able to scavenge and quench the ROS and thus modulate the intensity and extent of the stress response to greater or lesser degrees, based on their concentrations and radical scavenging efficiencies, and thus modify the Ca<sup>2+</sup> signature and ultimately the intracellular molecular responses.

**Keywords:** humic substances, humic acid, biostimulants, electron accepting capacity, electron donating capacity, mechanism of action, SFRC-semiquinone free radicals content

## INTRODUCTION

The size of the humic substance (HS) market, which is dominated by the agricultural and horticultural sectors, was 494.9 million USD in 2020 (Puldini and Pandey, 2020). The demand in these sectors is expected to grow at a compound annual growth rate of 12% to reach 610.5 and 235.7 M, respectively, by 2027. The increasing demand for HS has three dominant drivers. The first is the need to increase agricultural food production efficiencies in the face of continued increases in global population, urbanization, and industrialization, all of which decrease agricultural farmland and soil health (Puldini and Pandey, 2020). The second is the need to increase crop nutrient use efficiency to contend with limited fertilizer resources, for example, for P fertilizer (Alewell et al., 2020), and the stringent regulations that are increasingly imposed by governments on the use of inorganic fertilizers, the overuse of which leads to water and atmospheric pollution (Randeep et al., 2019). Finally, the impacts of climate change have produced modifications in temperature, rain fall, and drought patterns. This climate variation imposes abiotic stresses on plants, which exacerbate biotic stresses, both of which result in significant negative impacts on crop productivity (Onyekashi, 2019).

Humic substances are complex mixtures of thousands of different molecules that result primarily from the microbial breakdown of dead plant tissues. They occur in soils, composts, peats, spropels, and in brown, lignitic, and sub-bituminous coals (Lamar, 2020). They are composed of three different fractions operationally based on differing solubilities in strong acid and alkaline aqueous solutions (Stevenson, 1982). Humic acids (HA) are alkaline soluble and acid insoluble. Fulvic acids (FA) are soluble in both acid and alkaline solutions. The humin fraction is insoluble at all pH values. For production of commercial HS products for agricultural and horticultural purposes, the focus is primarily on HA and FA and they are almost exclusively obtained from particulate terrestrial sources, but also to a lesser extent, terrestrial aquatic sources (i.e., blackwater rivers). These particulate sources include various forms of coals including lignite, leonardite [i.e., oxidized lignite (OLG)], humalite and humate [i.e., both oxidized sub-bituminous coals (OSB)], and humic shales and mudstones. Humic acids are also obtained from different compost types including, most notably, vermicomposts (i.e., earthworm composts or feces). However, for production of commercial HS products, the preponderance are produced from OSBs and OLGs. HS are applied as dry ore that has been milled

to different size classes or as mostly liquid potassium (K-humate) and less frequently, ammonium (NH<sub>4</sub>-humate) products.

Humic substances are used as crop plant biostimulants because, under the right conditions, they elicit a metabolic reprogramming in plants (Roomi et al., 2018) that includes up-regulation of important metabolic processes like glycolysis and the tricarboxylic acid cycle (Conselvan et al., 2018), the antioxidant defense (Garcia et al., 2012; Roomi et al., 2018), and nutrient uptake systems (Quaggiotti et al., 2004), and they induce phenotypic changes primarily in root system architecture (see review by Nardi et al., 2021 and references therein). Metabolic reprogramming, which follows a mild stress response (i.e., eustress), primes plants to enable them to cope with biotic and abiotic stresses (Canellas et al., 2020), which inevitably occur during any growing season, and to maintain or improve productivity (Lenssen et al., 2019). Up-regulation of the antioxidant defense system is important to counterbalance the overproduction of reactive oxygen species (ROS) that occurs during the stress response (i.e., the oxidative burst) (Sewelam et al., 2016). ROS indiscriminately destroy proteins (e.g., enzymes and nutrient transporters), lipids (e.g., cell membranes), and nucleic acids (e.g., DNA and RNA) leading to reduced metabolic functioning or in extreme cases, death (Shah et al., 2001). HS applied to plants have been shown to up-regulate the production of antioxidant enzymes (e.g., superoxide dismutase, catalase) and non-enzymatic antioxidants (e.g., ascorbic acid, glutathione) that quench ROS, which eliminates or minimizes oxidative damage (Moghadam et al., 2014; Hemida et al., 2017). HS also up-regulate important proteins like plasma membrane (PM) H<sup>+</sup>-ATPases (Canellas et al., 2002), the activities of which provides the proton motive force for ion and solute transport into and out of cells (Bobik et al., 2010; Falhof et al., 2016). In addition, HS also up-regulate the genes responsible for production of transport proteins responsible for NO<sub>3</sub><sup>-</sup> (Quaggiotti et al., 2004), HPO<sub>4</sub><sup>-</sup> (Jindo et al., 2016) and Fe (Trevisan et al., 2010) uptake into root cells. Collectively, up-regulation of these types of proteins can result in increased nutrient use efficiency of N, P, and Fe, particularly in stressed plants (Monda et al., 2021).

Historically, in agricultural and horticultural applications, HS have been used as biostimulants using a “black box” approach, i.e., used without knowledge of what molecular structures are responsible for eliciting the plant biostimulant response (PBR). In order to optimize the design and effectiveness of HS-based products, to consistently enhance crop plant growth and productivity, the chemical structures responsible for elicitation of the PBR must be identified. A plethora of structure-activity relationship (SAR) studies, designed to elucidate the chemical nature of HS-elicited PBR, that is manifested in documented physiological and morphological changes, have been reported (Tables 1–3 and references cited therein). These studies have included applications of different types of un-fractionated and fractionated (e.g., fractionated by pH, molecular size, chemical modifications, and extraction in organic solvents) HAS from different sources (i.e., ores, soils, and vermicomposts), applications to a variety of monocot (e.g., *Zea mays* L. and *Oryza sativa* L.) and dicot (e.g., *Arabidopsis thaliana*) species use under various growth conditions (e.g., hydroponics, pot culture),

**Abbreviations:** ATR, attenuated total reflectance; DACC, depolarization activated calcium channels; EAC, electron accepting capacity; EDC, electron donating capacity; EEM, excitation emission matrix; ELG, Eocene brown coal; EPR, electron paramagnetic resonance; FA, fulvic acid; FI, fluorescence index; FT-ICR MS, Fourier transform ion cyclotron resonance mass spectrometry; FTIR, Fourier transform infrared; HA, humic acid; HB, hydrophobicity index; HS, humic substances; IAA, indole acetic acid; NMR, nuclear magnetic resonance; NOX, NADP(H) oxidase; OLG, oxidized lignitic coal; OSB, oxidized sub-bituminous coal; OXPHOS, oxidative phosphorylation; PBR, plant biostimulant response; PM, plasma membrane; PPM, plant plasma membrane; ROS, reactive oxygen species; SFRC, semiquinone free radical content; SUVA, specific ultraviolet absorbance; TEAC, Trolox equivalent antioxidant capacity; TPS, total percentage increase score.

**TABLE 1** | Review of structure/activity studies of ore-derived humic substances on plant morphological characteristics (A) and physiological parameters (B).

(A) Root Parameters								
Citation	# Lateral roots	Lateral root length	Lateral root density	Principal root length	Root Surface area	Root Diam.	Root hair density	Structural characteristics proposed to effect root parameters
David et al., 2014		+	+					Positive correlations between root growth and plant mass and molecular weight, but not aggregate size and between root growth and light absorbing groups
(B) Physiological Parameters								
	Enhanced NO <sub>3</sub> <sup>-</sup> uptake	Total plant carbohydrate and proteins						
Piccolo et al., 1992a	+							Preponderance of COOH groups and low molecular size fractions (i.e., <3500 Da)
David et al., 2014		+						Plant growth increment correlated to higher molecular weight HA fraction (70–100 kg mol <sup>-1</sup> )

**TABLE 2** | Review of structure/activity studies of soil-derived humic substances on plant root morphological characteristics (A) and physiological parameters (B).

(A) Root Parameters								
Citation	# Lateral roots	Lateral root length	Lateral root density	Principal root length	Root Surface area	Root Diam.	Root Dry Mass	Structural characteristics proposed to effect root parameters
Canellas et al., 2008					+		+	Positive correlations with FI, semiquinone-type free radical content, hydrophobic C; negative correlations with E4/E6, COOH acidity and total acidity.
Canellas et al., 2009	+			+			+	Hydrophobic domains that house hydrophilic molecules that can be released by the action of organic acids that are exuded by plants in response to HA
Muscolo et al., 2010	+	+						COOH-rich fraction decreased lateral root length but not number. Phenolic-rich fraction inhibited both.
Sleighter et al., 2015							+	Hydrophilic, more O-rich fractions had the greatest effect on enhanced shoot development. The hydrophobic, highly aromatic fractions had the greatest impact on enhanced root development.
(B) Physiological Parameters								
	H <sup>+</sup> -ATPase							
Canellas et al., 2008	+							Positive correlations with FI, semiquinone-type free radical content, hydrophobic C; negative correlations with E4/E6, COOH acidity and total acidity.
Canellas et al., 2009	+							Hydrophobic domains that house hydrophilic molecules that can be released by the action of organic acids that are exuded by plants in response to HA

and both root and foliar applications. However, a direct causal relationship between HS chemical structural features responsible for the elicitation of the PBR remains elusive. This is undoubtedly due in part to the chemical complexity of HS, the difficulty of isolating chemically defined fractions from HS super-complex

mixtures, and the possibility that various chemical structures in HS might be capable of elicitation of varied responses. From these studies, the primary conclusion is that low molecular weight hydrophilic molecules that are trapped in hydrophobic domains, when released to the soil solution, can interact with

**TABLE 3 |** Review of structure/activity studies of vermicompost humic substances on plant morphological characteristics **(A)** and physiological parameters **(B)**.

<b>(A) Root Parameters</b>								
Citation	# Lateral roots	Lateral root length	Lateral root density	Principal root length	Root Surface area	Root Diam.	Root hair density	Structural characteristics proposed to effect root parameters
Aguiar et al., 2009	+			+	+			Negative correlation between lateral root length and molecular weight. All other root parameters not effected by molecular weight. Concluded chemical structures more important than molecular weight.
Dobbss et al., 2010	+	+						No influence of molecular size. High correlation with hydrophobic index (HB/Hi)
Canellas et al., 2010	+	+	+	+		+	+	Unfractionated HA and all size fractions, in general enhanced the measured parameters. Molecular size not a primary factor. Chemical structure more important. Attributed activity to the heterogeneous, mobile molecules present in all size fractions including unfractionated HA.
Canellas et al., 2011	+							Argues that results support the theory that hydrophilic elements, protected by hydrophobic domains are responsible for induction of lateral root growth and auxin-like activity, once released due to molecular conformational changes.
Canellas et al., 2012	+							HB/Hi index and the HI index had the greatest positive effect on predicting increases in the numbers of lateral roots. HB index was negatively correlated with lateral root growth
Aguiar et al., 2013	+	+				+		Methyl, aryl, O-aryl (from lignin) and carboxyl had the greatest positive correlation to lateral root emergence. O-alkyl, di-O-alkyl (from carbohydrates and cellulose) and C-alkyl had negative correlations. Methyl, aryl, O-aryl and carboxyl positively correlated to root growth. Claim that carboxyl functional groups required for HS bioactivity.
Garcia et al., 2016		+				+	+	Root surface area, length in the 0.5–1.5 mm diam. class and to a lesser extent root length were associated with C-Alk (O) and C-COOH. Growth of larger root diameter classes 1.5–3.5 mm and >3.5 mm were associated with C-Ar, Arom., and C-Alk (di-O).
<b>(B) Physiological Parameters</b>								
	Enhanced Nitrate uptake	H <sup>+</sup> -ATPase Activity	Medium acidification	Enhanced phenyl-propanoid metabolism	Auxin-like activity			Structural characteristics proposed to effect physiological parameters
Piccolo et al., 1992a	+							Preponderance of COOH groups and low molecular size fractions (i.e., <3500 Da)
Canellas et al., 2008		+						Positive correlations with FI, semiquinone-type free radical content, hydrophobic C; negative correlations with E4/E6, COOH acidity and total acidity.
Canellas et al., 2009		+						H <sup>+</sup> -ATPase activity correlated with LRM which included HB/Hi, MW and %C <sup>1</sup>
Schiavon et al., 2010								Combination of HMW HA and IAA-effects could not be separated.
Dobbss et al., 2010		+						No influence of molecular size. Hydrophobic index (HB/Hi) was highly correlated with increases in lateral root growth and H <sup>+</sup> -ATPase activity.
Canellas et al., 2010		+						Unfractionated HA and all size fractions, in general enhanced the measured parameters. Molecular size not a primary factor. Chemical structure more important. Attributed activity to the heterogeneous, mobile molecules present in all size fractions including unfractionated HA.
Canellas et al., 2011					+			Argues that results support the theory that hydrophilic elements, protected by hydrophobic domains are responsible for induction of lateral root growth and auxin-like activity, once released due to molecular conformational changes.
Canellas et al., 2012		+						HB/Hi index and the HI index
Aguiar et al., 2013			+					Methyl, aryl, O-aryl (from lignin) and carboxyl had the greatest positive correlation to lateral root emergence. O-alkyl, di-O-alkyl (from carbohydrates and cellulose) and C-alkyl had negative correlations. Medium acidification closely associated with lateral root emergence.

the plant plasma membrane (PPM) or enter the cytoplasm and elicit the PBR.

Many of the HS SAR studies have employed  $^{13}\text{C}$ -NMR and Fourier transform infrared (FTIR) spectroscopies combined with plant morphological and or physiological parameters in various chemometric analyses to attempt to identify relationships between HS chemical structure and morphological and physiological responses in plants. These studies have revealed some important clues, as mentioned above. However, HS are redox-active organic compounds and two very important attributes of HS that these analytical techniques do not directly measure are their electron-accepting capacities (EAC, pro-oxidant activity) and electron-donating capacities (EDC, antioxidant activity) (Lamar, 2020). EAC originates primarily in HS quinonoid structures (Scott et al., 1998; Aeschbacher et al., 2011) and EDC in phenolic structures (Aeschbacher et al., 2012). Aeschbacher et al. (2012) reported on work in which they compared the relative EAC and EDC of HA and FA from terrestrial and aquatic sources. They found, in general, that the EAC of HA is greater than those of FA, terrestrial particulate HA sources have greater EAC than aquatic sources, and EAC is highly correlated to degree of aromaticity. Conversely, the EDC of terrestrial HA and FA are of similar magnitude and not strongly correlated to aromaticity. Aquatic HS tend to have greater EDC than terrestrial particulate sources, and their EDC is strongly correlated to aromaticity. Given the redox-driven nature of the plant stress-response, it is reasonable to suggest that the ability of HS to accept and donate electrons (i.e., act as electron shuttles) is involved in the PBR at some level. Indeed, in one SAR study, soil HA EAC was indirectly measured by assessing the semiquinone-type free radical content (SFRC) and fluorescence index (FI,  $A_{465nm}$ ) (Canellas et al., 2008). FI was significantly and positively correlated to SFRC of soil HA (Milori et al., 2002). Both the SFRC and FI were found to be significantly and positively correlated to root dry mass, area, and  $\text{H}^+$ -ATPase activity (Canellas et al., 2008). Also, in the mid-20th century, Flaig and Otto (1951) who were working with water cress, demonstrated that hydroxyanthraquinones, in particular, alizarin (1,2-dihydroxyanthraquinone) and quinalizarin (1,2,5,8-tetrahydroxyanthraquinone) applied at a concentration of  $1 \times 10^{-6}$  g  $\text{ml}^{-1}$ , stimulated root growth, by 28.9 and 27.9%, respectively, relative to controls. Interestingly, various molecular weight fractions obtained by dialysis (i.e., <3,500 Da and 3,500–14,000 Da) of several International Humic Substances Society (IHSS) standard HAs were found to contain high concentrations of quinones relative to the bulk HA, based on reducing capacity per gram of C (Yang et al., 2016). Based on these results, the effect(s) of electron shuttle activities of HA on the PBR deserve further investigation. A good portion of the work on SAR of HS has been done with HA obtained from earthworm feces or vermicompost (Table 3). The HA from these sources and forest soils (Pizzeghello et al., 2001) have been reported to contain physiologically relevant concentrations of the plant growth hormone indoleacetic acid (IAA) (Muscolo et al., 1998, 2009; Trevisan et al., 2010; Schiavon et al., 2010). The presence of IAA in vermicompost and forest soils is not surprising, because these sources promote the growth of microbial populations that harbor biosynthesis capacity for IAA and other growth regulators

(Spaepen and Vanderleyden, 2011). The presence of IAA in HA from these sources may confound attempts at identifying the structures in HA that are responsible for initiating the PBR. IAA has not been found in HA obtained from terrestrial ore sources, for example, leonardite coals (Aguirre et al., 2009; Mora et al., 2010, 2014a,b; Jannin et al., 2012; Olaetxea et al., 2015). Therefore, studies employing HA obtained from coal sources are more relevant to defining the mode-of-action of HA used for agricultural purposes.

Oxidized sub-bituminous coals and OLG coals evolved from ancient peat beds that formed during the Cretaceous period. Younger brown coals (e.g., ELG) evolved from peat beds that formed during the middle to late Eocene epoch (Holdgate et al., 2000). Cretaceous and Eocene peat beds developed under different types of vegetation, environmental conditions, and inundations from a variety of inorganic contaminants (e.g., wind-blown silt, volcanic ash, sediments from spring floods, etc.), all of which could vary spatially and temporally. They were also subjected to different temperatures and pressures during the process of coalification after burial. Because of this great diversity of developmental factors, coal chemistry (e.g., degrees of aromaticity compared to aliphaticity) varies significantly between and within coal seams (Warwick, 2005). As a result, the chemistry also varies among HAs obtained from coals from different sources. Therefore, examining the PBR effects of HA from a variety of different sources, which possess varying chemistries and that are extracted, purified, and structurally defined based on a variety of analytical techniques, might provide an effective tool when analyzed along with plant physiological and/or morphological parameters using chemometric techniques, to provide more insight into the SAR of the HA-elicited PBR.

The objectives of this research were (1) to extensively chemically characterize HA purified from four different OSB ore sources, two OLG ore sources, and one Eocene brown ore source (ELG). Analytical characterization was accomplished using  $^{13}\text{C}$ -NMR,  $^1\text{H}$ -NMR, FTIR, Fourier transform ion cyclotron resonance mass spectrometry (FT-ICR MS), ultraviolet/visible (UV/VIS) and fluorescence spectroscopies, electron spin resonance (EPR) spectroscopy to determine semiquinone-type free radical content (SFRC), EAC and EDC, and antioxidant capacity (TEAC); (2) to evaluate the effects of the purified HA on early corn seedling shoot and root growth and morphology in bioassays; and (3) to use chemometric analysis combining the HA analytical data and plant morphological and biomass data from the bioassays, attempting to identify HA chemical characteristics that might be responsible for inducing plant morphological changes produced by the HA treatments.

## MATERIALS AND METHODS

### Test Materials

The HAs used in this investigation were extracted and purified from four Cretaceous OSB sources from three locations throughout the western United States and one from western Canada; two Cretaceous OLG sources, including one from the western United States and one from central Europe, and a humic

product produced from middle to late Eocene brown coal (ELG) from Australia (Table 4).

## Extraction and Purification of Humic Acids

The HAs investigated in this study were all extracted according to the new standardized method (Lamar et al., 2014). Briefly, for each HA, about 50 g of each ore was milled to pass a 60-mesh sieve. Each milled HA (2.5 g) was extracted in 1 L 1 M NaOH for 6 h under N<sub>2</sub>. After extraction, the entire volume was centrifuged at 4,300 rpm for 5 min to remove insoluble material. The alkaline supernatant was then transferred to a 1 L Erlenmeyer flask and acidified to pH 1 with 37% HCl to precipitate the HA. After ca. 2 h to allow full precipitation of the HA, the entire volume was centrifuged at 4,300 rpm for 30 min. After centrifugation, the supernatant (i.e., the fulvic fraction) was decanted, and the precipitated HA was transferred to a 250 ml centrifuge tube. The HA was then de-ashed using 200 ml of a dilute HCl/HF solution [(5 ml HCl 36% + 5 ml HF 48%) L<sup>-1</sup>]. After the HCl/HF treatment, the HA was washed twice with DI H<sub>2</sub>O acidified to pH 1 with concentrated HCl. After washing, the purified HA were suspended in 50 ml DI H<sub>2</sub>O, frozen at -80°C, and lyophilized. Each lyophilized HA was then stored in a 50 ml centrifuge tube in a desiccator under vacuum until use.

## <sup>13</sup>C- and <sup>1</sup>H-NMR Analysis

The HA samples were analyzed by solid-state <sup>13</sup>C cross polarization magic angle spinning (CPMAS) NMR spectroscopy on a Bruker AV300 spectrometer equipped with a 4 mm wide-bore MAS probe. The NMR spectra were obtained by applying the following parameters: 5,000 Hz of rotor spin rate; 2 s of recycle time; 1H-power for CP 92.16 W; 1H 90° pulse 2.85 μs; <sup>13</sup>C power for CP 150.4 W; 1 ms of contact time; 30 ms of acquisition time; 4,000 scans. Samples were packed in 4 mm zirconium rotors with Kel-F caps. The cross-polarization pulse sequence was applied with a CP/TOSS (total sideband suppression) sequence and with a composite shaped “ramp” pulse on the 1H channel in order to account for the inhomogeneity of Hartmann-Hann condition at high rotor spin frequency. The Fourier transform was performed with 4k data points and an exponential

apodization with 100 Hz of line broadening. The main carbon functionalities were grouped into the following chemical shift regions: aliphatic-C: 0–35 ppm; complex aliphatic C: 35–50 ppm; methoxyl-C: 50–60 ppm; O-alkyl (carbohydratic)-C: 60–96 ppm; anomeric-C: 96–108 ppm; aromatic I-C: 108–120 ppm, aromatic II-C: 120–145 ppm; phenolic-C: 145–162 ppm; carboxyl-C: 162–190 ppm; and ketonic-C: 190–216 ppm. The relative contribution of each region was determined by integration (ACD Labs Spectrus Processor 2015.2.5 software) and expressed as percentage of the total area.

The eight HA samples were also analyzed using <sup>1</sup>H NMR. The liquid-state <sup>1</sup>H-NMR spectra were obtained on a 400 MHz Bruker Biospin Avance III NMR equipped with a broadband inverse (BBI) probe. The HA samples were dissolved at ca. 100 mg C L<sup>-1</sup> in sodium deuteroxide (NaOD) in deuterium oxide (D<sub>2</sub>O) that was diluted to pH 9 with ultrahigh quality (UHQ) water. All samples were then minimally diluted further to give a final sample concentration of 90:10 H<sub>2</sub>O:D<sub>2</sub>O. The <sup>1</sup>H NMR spectra were obtained using a water suppression pulse program (WATERGATE pulse sequence, Lam and Simpson, 2008) and acquired with a 1 ms recycle delay and a time domain of 16k. The spectra were acquired using 1000 scans giving a 1 h analysis time. The scans were co-added and the summed free induction delay (FID) signals were exponentially multiplied and zero-filled once. Spectra were processed with a line broadening of 10 Hz. Peaks were integrated and their resulting areas determined. Tetramethylsilane (yielding a peak at 0.0 ppm in the spectra) was included in to the D<sub>2</sub>O as a calibration standard.

## Attenuated Total Reflectance-Fourier Transform Infrared Spectroscopy

Infrared spectra were obtained with a Perkin-Elmer Spectrum Two FTIR spectrometer in attenuated total reflectance (ATR) mode. Freeze dried samples were loaded onto the diamond crystal and clamped to a consistent loading of 92 N. All spectra were acquired using 50 scans at a resolution of 4 cm<sup>-1</sup> from 4,000 to 450 cm<sup>-1</sup> in absorbance mode. Scans were smoothed, ATR corrected, and baseline adjusted using Perkin-Elmer Spectrum software.

**TABLE 4** | Percentages of HA and ash in ore or products and elemental analysis of the purified seven humic acids.

Humic Acid Sample	Ore Analysis		Purified HA elemental analysis <sup>C</sup>				
	HA <sup>B</sup>	Ash <sup>B</sup>	C	N	H	S	O
OSB1	61.18	26.26	59.02	1.71	3.45	0.17	29.76
OSB2	47.11	39.38	57.51	1.46	3.52	0.24	33.27
OSB3	69.68	11.14	61.27	1.80	3.50	0.32	27.79
OSB4	61.86	28.83	59.36	1.77	3.55	0.33	31.05
OLG1	61.26	17.16	55.99	1.22	3.55	0.27	30.16
OLG2 <sup>A</sup>	72.31	15.52	59.87	1.42	3.85	0.37	28.33
ELG	76.65	6.54	58.49	0.83	3.72	0.47	30.73

<sup>A</sup>The OLG2 HA was extracted from a granulated K-humate that was produced from an OLG ore.

<sup>B</sup>Percent HA and ash were determined using the methods described in Lamar et al. (2014).

<sup>C</sup>Elemental analyses were conducted on a Thermo Scientific FlashSmart CHNS/O analyzer using purified HAs.

## Ultraviolet/Visible and Excitation Emission Matrix Analysis

Ultraviolet/visible absorbance values were measured simultaneously as EEM spectra were acquired on a spectrophotometer equipped with a CCD detector (Aqualog®; Horiba Instruments, NJ, United States) with an excitation range of 240–500 nm at 3 nm intervals and an emission range of 213–623 at 3.368 nm intervals, with an integration time of 1 s. All samples were analyzed at a range of TOC values (0.5–6 mg C L<sup>-1</sup>) as measured by high temperature catalytic combustion to CO<sub>2</sub> on a Shimadzu TOC-V<sub>csn</sub> total organic carbon (TOC) analyzer. Specific UV absorption at 254 nm (SUVA<sub>254</sub>) was calculated based on dividing the absorbance at 254 nm by the TOC (mg L<sup>-1</sup>) and multiplying the quotient by 100 (Spenser et al., 2012). Higher SUVA<sub>254</sub> values indicate higher aromatic content (Weishaar et al., 2003) and molecular weight (Chowdhury, 2013). The fluorescence index (FI) was calculated from the ratio of emission intensity at 470:520 nm at an excitation of 370 nm (Cory and McKnight, 2005). Low FI values indicate a more terrestrial nature. Fluorescence components were determined as humic-like Peak A (integrated area at 240–300 nm EX, 400–600 nm EM), humic-like Peak C (integrated area at 300–360 nm EX, 400–600 nm EM), and peptide-like Peak T (integrated area at 240–300 nm EX, 250–350 nm EM) (Fellman et al., 2010).

## Analysis of Electron Accepting Capacity and Electron Donating Capacity of Humic Acids

For EAC and EDC analysis, approximately 6 mg of each HA sample was weighed into a 250 ml beaker. The samples were then transferred into an anoxic glove box under a pure N<sub>2</sub> atmosphere. Six milliliters of 0.1 M phosphate buffer at pH 7.0 with 0.1 M KCl was added to each sample. The mixtures were stirred and slightly sonicated until analysis. Mediated electrochemical analyses, i.e., mediated electrochemical reduction (MER) and mediated electrochemical oxidation (MEO) were then performed as outlined in Aeschbacher et al. (2010). Triplicate analyses were conducted for each HA, and the data were analyzed by ANOVA. Differences among means were detected using Tukey's test ( $\alpha = 0.05$ ).

## Electron Spin Resonance Spectroscopy: Determination of Semiquinone-Type Free Radical Content

Electron spin resonance (ESR) spectra were obtained with an Active Spectrum MicroESR spectrometer operating at X-band frequencies at room temperature for liquid samples in 2 mm (i.d.) × 100 mm thin-walled quartz tubes (Wilmaad-LabGlass, Vineland, NJ). Each freeze-dried HA was prepared by dissolving ca. 150 mg in 25 ml of 0.1 M NaOH. Spectra were recorded at 25°C using the following conditions: Microwave power, 1 mW; modulation coil amplitude, 80%; sweep field, 3,425–3,550 G; frequency 9782.66 MHz; RF power, 13.75 dBm, 100 scans and 2,800 points. Second derivative spectra were the average of 100 scans, which were automatically baseline corrected using

Active Spectrum Micro-ESR Analysis and Processing Software. The SFRC of the HA were quantitated using 4-hydroxy tempo (Tempol, Sigma Chemical Co.) as a spin standard. A 100 mM solution of Tempol in 0.1 M NaOH was prepared and used to make 5, 10, 20, and 40  $\mu$ M dilutions with 0.1 M NaOH. A standard curve was prepared by plotting the double integral for each dilution from baseline corrected spectra against Tempol concentration. The Tempol concentration corresponding to the double integral of each HA was then used to determine the SFRC. The HA [SFRC] was then divided by the mg of HA to give SFRC. Mg<sup>-1</sup>. Triplicate analyses were conducted for each HA, and the data were analyzed by ANOVA. Differences among means were detected using Tukey's test ( $\alpha = 0.05$ ).

## Fourier Transform Ion Cyclotron Resonance Mass Spectrometry Analysis

Electrospray ionization (ESI) coupled to Fourier transform ion cyclotron resonance mass spectrometry (FTICR-MS) provides molecular-level details about the organic matter composition of samples. The HA samples were dissolved at ca. 100 mg C L<sup>-1</sup> in ammonium hydroxide (NH<sub>4</sub>OH) at pH 9 with UHQ water. Samples were diluted further by a factor of 4 to give a final sample composition of 1:1 H<sub>2</sub>O:MeOH and were continuously infused into an Apollo II ESI ion source of a Bruker Daltonics 12 Tesla Apex Qe FTICR-MS. Samples were introduced by a syringe pump operating at 120  $\mu$ l h<sup>-1</sup>, and ESI voltages were optimized for each analysis. Ions were accumulated for 3–4 s in a hexapole before being transferred to the ICR cell, where 300 transients, collected with a 4 MWord time domain, were added, giving analysis times of 37–42 min total. The summed FID signal was zero-filled once and Sine-Bell apodized prior to fast Fourier transformation and magnitude calculation using the Bruker Daltonics Data Analysis software.

Numerous peaks were detected at each nominal mass, indicating the complexity of the samples. Prior to data analysis, all samples were externally calibrated with a polyethylene glycol (PEG) standard and internally calibrated with fatty acids, dicarboxylic acids, and other naturally present ions within the sample (Sleighter et al., 2008). The ultrahigh resolving powers of the FTICR-MS are capable of separating m/z values to a mass accuracy of less than 1 ppm. A molecular formula calculator generated empirical formula matches using carbon, hydrogen, oxygen, nitrogen, and sulfur: (C<sub>5–50</sub>H<sub>5–100</sub>O<sub>1–30</sub>N<sub>0–4</sub>S<sub>0–2</sub>). Only m/z values with a signal to noise (S/N) ratio above 3 were inserted into the formula calculator. The assigned formulas, in the vast majority of cases, agreed within an error value of <0.5 ppm compared to the calculated exact mass of the determined formulas. Using this criteria, 84–94% of peaks are assigned formulas, which accounts for 88–97% of the total spectral magnitude (excluding contributions from <sup>13</sup>C isotopes). The mass spectra and molecular formula assignments were found to be reproducible, and the various samples were notably different from one another when compared to instrumental duplicates of the same sample (Sleighter et al., 2012). To ensure that the instrument was working appropriately, Suwannee River FA obtained from the International Humic Substances Society

(IHSS), which was dissolved at 50 mg C L<sup>-1</sup> in UHQ water, was analyzed at a final composition of 20 mg C L<sup>-1</sup> in 1:1 H<sub>2</sub>O:MeOH. From the formula assignments, the magnitude-weighted O/C and H/C averages were 0.50 and 1.07, respectively, which are within the suggested metrics presented by Hawkes et al. (2020). For molecular-level comparison to the HA extracted here, leonardite HA from the IHSS was also analyzed, according to the same procedure used for the seven HAs described above.

## Antioxidant Analysis—Trolox Equivalent Antioxidant Capacity

The method used was based on the capacity of the purified HAs to inhibit the ABTS radical (ABTS<sup>+</sup>) by using Trolox as a reference antioxidant standard, as described by Re et al. (1999) and modified by Mingle and Newsome (2020). The ABTS<sup>+</sup> radical was generated by a chemical reaction of 25 ml of ABTS (0.7 mM) with 25 ml K<sub>2</sub>S<sub>2</sub>O<sub>8</sub> (2.45 mM) and allowed to stand in darkness at room temperature for 1 h to allow the formation and stabilization of the radical. The working solution was prepared by taking a volume of the radical solution and diluting it in methanol until its absorbance at 734 nm was 0.70 ± 0.03. The standard calibration curve was obtained using 5 points of Trolox dilutions (0–50 μM). Several concentrations for each HA were assayed to determine the optimal one (20 mM C L<sup>-1</sup>). For the assay, 2 ml of the ABTS<sup>+</sup> diluted solution and 100 μl of either the sample or the standard solution were added to the measuring cuvette and thoroughly mixed for 30 s, then the absorbance was measured at 734 nm in a Shimadzu UV-1800 spectrophotometer (Shimadzu, Japan). An inhibition percentage in the range 20–80% was achieved. Each sample was analyzed in triplicate. The results were expressed as μmol of Trolox equivalents per ml of HA solution.

## Plant Material and Bioassay Growing Conditions

A series of four bioassays were conducted in which the effects of HAs on corn seedlings were evaluated. Corn seeds were surface sterilized by mixing seeds in 4% hypochlorite solution for 0.5 h. Seeds were then rinsed five times with sterile DI H<sub>2</sub>O. Seeds were germinated for 2 days in dark conditions at room temperature (23°C) on sterile solid media containing Murashige and Skoog (MS) supplemented with 0.9% agar and 1% sucrose. Germinated seeds with radicals 20 mm (OSB1 and OLG1 HAs), 37 mm (OLG2 and ELG HAs), 17.5 mm (OSB2 and OSB4 HAs), and 16.5 mm (OSB3 HA) long were selected and transferred onto a floating circular foam disk within a 38 mm × 200 mm test tube containing 50 ml of 2 mM CaCl<sub>2</sub>. The foam disks had a hole in the middle which was large enough to insert the radical through but small enough to retain the seed. Radicals and the developing root systems were covered from the top by the foam disk and on the sides by placing the tubes into a styrofoam block that had holes drilled to a depth to cover the inserted tubes up to the level of the foam disk. There were 10 plants per treatment. Prior to use, a mixture of each HA in 0.1 M K phosphate buffer at pH 7 was prepared and the %C of each mixture was determined. These solutions were then used to prepare 600 ml of each HA at a concentrations of 8 mM C L<sup>-1</sup> in 2 mM CaCl<sub>2</sub>. HA mixtures were

pasteurized under nitrogen gas for 0.5 h at 65.6°C before adding them to the CaCl<sub>2</sub> solution. Control plants were grown in sterile 2 mM CaCl<sub>2</sub>. Plants were grown at 23°C under a photoperiod of 16 h of light and 8 h of dark for 7 days on a shaker at 30 rpm. On the seventh day, plants were removed from the test tubes for morphological analysis. Several plants that were contaminated (visually determined) were excluded from the analysis.

## Analysis of Plant Morphological Parameters

After removing plants from the test tubes, roots were gently rinsed and separated from shoots by cutting with scissors at the visually determined point of chlorophyll production. Rinsed roots were scanned and their morphology was analyzed using WinRHIZO software (Regent Instruments Canada Inc.). Morphological parameters evaluated included total root length (TRL), root surface area (RSA), and TRL according to these three diameter classes: 0–0.5 mm (TRL-F), 0.5–1 mm (TRL-M), and 1–1.5 mm (TRL-L). Leaves were separated from shoots by cutting where the leaf directly extended from the shoot. Leaves were scanned and analyzed using WinRHIZO software. The parameters measured were total leaf length (LL) and leaf surface area (LSA). After scanning, leaves and shoots were placed in small coin envelopes for dry weight analysis. Roots and shoots in coin envelopes were dried in a drying oven at 70°C for 1 week, followed by dry weight determination. Root and shoot dry weight (RDW and SDW), total dry weight (TDW), and morphological data were normalized by expressing as percent change from control. In this experiment, outliers for each parameter were determined using inner and outer quartiles. Any plant with more than four outliers was completely removed from the data set. All parameters were expressed as percent difference relative to controls. Data obtained were subjected to ANOVA using the Excel QI Macros plugin based on a significance level of α = 0.05. Significant differences among means were detected using Tukey's test at a significance level of α = 0.05.

## Chemometric Analyses and Molecular Mixing Model

A principal component analysis (PCA1) was conducted on a group of HA analytical data that included: %C in defined chemical shift regions from <sup>13</sup>C-NMR and HB (hydrophobic index); EAC, EDC, and EAC/EDC; SFRC (number of spins g<sup>-1</sup> from ESR spectroscopy), TEAC; SUVA (from UV/VIS spectroscopy); and FI (from fluorescence spectroscopy). The PCA was run using OriginPro 2021b software (OriginLab Corp., Northampton, MA, United States), which automatically normalizes the data using 0–1 normalization.

A second PCA analysis (PCA2), also using the OriginPro 2021b software, was conducted on the same HA analytical data described in PCA1 but with the addition of the plant biomass and morphological data, from the corn seedling bioassay experiments, that are shown in **Table 5**. Again, the data were normalized using the 0–1 method prior to PCA.

Mathematical algorithms were applied to the <sup>13</sup>C-NMR data to extract relevant quantitative information according to the

**TABLE 5** | Effect of seven HAs applied at 8 mM C L<sup>-1</sup> based on percent increase relative to the control for 10 plant parameters<sup>A</sup>.

HA	TDW	SDW	LL	LSA	RDW	TRL	RSA	TRL 0–0.5	TRL 0.5–1	TRL 1.0–1.5	TPS
OSB1(8) <sup>B</sup>	39.01 b	45.55 c	18.18 bc	12.77 d	15.53 b	<b>170.57 a</b>	73.89 cd	<b>320.43 a</b>	51.04 bc	46.22 abc	793.19
OSB2(8)	54.29 ab	124.80 ab	17.86 c	44.25 bcd	14.27 b	92.30 c	90.97 bc	135.59 cd	38.02 c	60.79 ab	673.14
OSB3(9)	<b>83.94 a</b>	89.09 b	<b>56.91 a</b>	<b>129.82 a</b>	<b>74.96 a</b>	<b>163.01 a</b>	<b>127.28 a</b>	213.03 b	68.14 abc	<b>98.14 a</b>	<b>1104.32</b>
OSB4(7)	<b>89.67 a</b>	<b>133.91 a</b>	<b>73.66 a</b>	122.85 ab	<b>59.93 a</b>	129.41 abc	<b>128.80 a</b>	170.61 bcd	<b>98.96 a</b>	<b>90.79 a</b>	<b>1098.58</b>
OLG1(9)	30.45 b	49.85 c	11.70 c	3.71 d	22.03 b	114.37 bc	42.16 d	210.10 bc	30.94 c	13.04 c	528.35
OLG2(9)	46.24 ab	38.16 c	48.14 ab	42.62 bcd	<b>61.74 a</b>	139.78 ab	116.06 ab	186.39 bcd	89.11 ab	29.69 c	798.11
ELG(6)	28.12 b	34.81 c	24.48 bc	13.64 d	16.50 b	85.84 c	80.07 c	124.78 d	41.09 c	13.28 c	462.61

Means within columns followed by the same letter are not significantly different by LSD multiple comparison procedure at  $\alpha = 0.05$ . Means in bold type indicate the largest significant increase relative to the control.

<sup>A</sup>Percent increase relative to the control, for each parameter, was determined by the following formula: [(parameter value of treated seedling – parameter value of the average of 10 control seedlings)/parameter value of treated seedling]  $\times$  100. The percent increase relative to control values for each treated seedling were then used in an ANOVA for each parameter. For the OSB1 and OLG1, OSB2 and OSB4, the ELG and OLG2 and the OSB3 bioassays there were 8, 9, 10, and 8 control replicates.

<sup>B</sup>Numbers in parenthesis indicate numbers of treated plants used in the ANOVA.

molecular mixing model developed by Baldock et al. (2004) and modified by Hockaday et al. (2009). Briefly, NMR peak areas were used to estimate the relative proportion of five components that represent the major biomolecule classes found in natural organic matter to describe the molecular composition of the sample. The five classes corresponded to: carbohydrate, protein, lignin, lipid, and condensed aromatic structures (CAS). The model was built on the empirical data obtained for terrestrial environments. The linear combination of the five components allowed the model to calculate the best fit to the measured NMR area distribution.

From the <sup>1</sup>H-NMR analysis, the raw NMR spectra at 0.5–11 ppm were exported for each sample from the instrument at the resolution at which the NMR records data. This data export gives an intensity value every 0.0008 ppm, yielding 13,225 data points per sample. This level of resolution is unnecessary and leads to datasets that are much larger than most computers can handle. Thus, using an in-house written MatLab code, each spectrum was averaged across every 5 data points, giving a new resolution of 0.004 ppm. In order to remove pH bias that can shift the chemical shifts for small molecular weight organics (i.e., acetate/acetic acid and formate/formic acid), the following regions were deleted prior to executing PCA: >8 ppm, 3.2–4 ppm, and 1.8–2.4 ppm (Sleighter et al., 2015). Data were normalized for each sample so that the summed total intensity equaled one for all samples. These 1,535 intensity values at each ppm were utilized as variables in the NMR PCA.

For PCA of the FTICR-MS data, a list of variables was created from all CHO and CHON formulas that were assigned to the seven ore HAs and the IHSS leonardite HA, yielding a unique list of 6,111 formulas. About 22.6% (1,379) of these formulas were detected in all eight samples, while 22.9% (1,401) were unique to only one sample. The relative magnitudes for each corresponding formula were normalized for each sample so that the summed total magnitude equaled one for all samples.

The FTIR spectra of the seven ore-derived HA were converted to their second derivative spectra using OriginLab Pro 2021b software. In order to gain more insight into differences between the HAs that promoted fine root growth to greater percentages increases relative to controls (i.e., the OSB1, OSB3, and OLG1

HAs) than the remaining HAs (with the exception of the OLG2 HA that was very different chemically) a technique, developed by Jimenez-Gonzalez et al. (2019), was used. The original spectra were subjected to a resolution enhancement technique, which involved multiplying the second derivative of each spectrum by 1,500 and then subtracting the modified second derivative spectra from the original spectra (Almendros et al., 1992). Using these resolution enhanced spectra, average spectra for the OSB1/OSB3/OLG1 HAs (TRL-F<sup>++</sup>) and the OSB2/OSB4/ELG HAs (TRL-F) were calculated. The difference spectrum (TRL-F<sup>++</sup> – TRL-F) was then calculated. To identify peaks that predominated in the TRL-F<sup>++</sup> spectrum, the TRL-F<sup>++</sup> was multiplied by a factor, in this case 1.22, identified by determining what value was required to make the difference equal to zero at the most negative peak in the 700–1,800 cm<sup>-1</sup> range, in the difference spectrum. This new difference spectrum, that highlighted the TRL-F<sup>++</sup> HA peaks, was then calculated using the formula 1.22(TRL-F<sup>++</sup>) – TRL-F. Finally, to identify peaks that predominated in the TRL-F HAs, the TRL-F spectrum was multiplied by a factor, in this case, 0.89, that was identified by determining the value that would make the most positive peak in the difference spectrum, in the spectral range between 700 and 1,800 cm<sup>-1</sup>, equal to zero. The difference spectrum that emphasized the peaks present in the TRL-F HAs were then produced using the formula –1[0.89(TRL-F<sup>++</sup>) – TRL-F].

## RESULTS

### Analysis of Ore Humic Acid and Ash Concentrations and Elemental Analyses of Purified Humic Acid

With the exception of the OSB2 ore, all of the ore sources had HA greater than 60%, with the highest HA, concentrations almost 77%, in the ELG ore. These high HA concentrations are the reason these ore sources are used for commercial production of humate products (Table 4). The OLG2 HA source was a product, and this explains the high HA concentrations and low ash content. The ELG ore was the youngest ore source and thus had not been exposed to the coalification process as long

as the OLGs and OSBs, explaining its comparatively high HA concentrations. The primary variability in the elemental analyses among the HAs was in the %C and %N. With the exception of the OSB2 HA, the OSB HAs had higher %C than did the other sources, which is expected as the %C increases and %O decreases as the process of coalification proceeds. However, because these are all oxidized coals, the re-oxidation process has the effect of decreasing the %C and increasing %O concentrations in the oxidized OLGs and OSBs (Yohe, 1958). In fact, the OSB2 HA had the highest %O.

## Electrochemical Analysis of Electron Accepting Capacity and Electron Donating Capacity, Electron Paramagnetic Resonance Analysis of Semiquinone Free Radical Content, and Trolox Equivalent Antioxidant Capacity Analysis

Electrochemical analysis revealed significant differences among the seven HAs for both EAC and EDC (Table 6). EACs of the OSB1 and OSB4 HAs were significantly greater than all other HAs, except OLG1 HA (Table 6). With the exception of OLG1 HA, the EACs of the OSB HAs were higher than the OLG2 and ELG HAs. The EDCs of the HAs from highest to lowest were ELG > OSB4 = OSB2 > OLG1 > OLG2 = OSB1 = OSB3. It was not surprising that the ELG, being the geologically youngest ore, had the highest EDC. The EAC/EDC represents the pro-oxidant to antioxidant capacity of the HAs. From highest to lowest EAC/EDC, the HAs ranked as follows: OSB1 > OSB3 > OLG1 > OLG2 > OSB4 > OSB2 > ELG. The OSB1, OSB3, and OLG1 HAs had a significantly greater SFRC than did the other HAs (Table 6). The HA with the lowest SFRC was OLG2 HA. The OSB1, OSB3, and OLG1 HAs had significantly higher numbers of semiquinone-type free radicals than the remaining HAs (Table 6). Based on the ABTS antioxidant assay, the antioxidant capacities of

**TABLE 7** | SUVA<sub>254</sub> and FI values for the seven ore-derived HAs.

Humic Acid Sample	SUVA <sub>254</sub> <sup>A</sup>	FI <sup>B</sup>
OSB1	11.1	0.91
OSB2	11.5	0.92
OSB3	11.9	1.04
OSB4	10.1	0.98
OLG1	10.1	0.95
OLG2	12.7	0.87
ELG	10.5	0.90

<sup>A</sup>SUVA, the specific UV absorbance at 254 nm/[C].

<sup>B</sup>FI, Ratio of emission intensity at 470:520 nm at an excitation of 370 nm.

the seven ore-derived HA were from greatest to smallest: OSB2 > OLG1 > OSB4 > ELG > OSB1 > OLG2 = OSB3.

## Ultraviolet/Visible and Fluorescence Analysis

Results for SUVA<sub>254</sub> and FI are given in Table 7. Higher SUVA<sub>254</sub> typically indicate a higher aromatic quality. However, when compared to the aromaticity values from the <sup>13</sup>C-NMR analysis, the SUVA<sub>254</sub> index was not highly correlated to aromaticity. The FI index was developed to distinguish terrestrial (i.e., plant-derived HS) from microbial-derived HS, with lower values indicating a more terrestrial nature (McKnight et al., 2001). However, the FI has been shown from PARAFAC analysis to be accounted for primarily by partially (i.e., semiquinones) reduced quinones (Cory and McKnight, 2005) and was strongly associated with EAC in the PCAs described below (Section 3.12). This is consistent with the EAC of HA originating in quinones (Aeschbacher et al., 2011). Characteristics calculated from the UV/VIS and EEMs analysis are given in Supplementary Table 1 and UV/VIS and EEMs spectra are shown in Supplementary Figures 1,2 in the supporting information. The humic-like Peak A and C fluorescence area integrations are shown in Supplementary Figure 3.

**TABLE 6** | EAC/EDC ratios and mean<sup>A</sup> EAC, EDC, SFRC, and TEAC values of the HAs.

Humic Acid Sample	EAC <sup>B</sup> (mmol g <sup>-1</sup> )	EDC <sup>B</sup> (mmol g <sup>-1</sup> )	EAC/EDC	SFRC <sup>C</sup> (spins g <sup>-1</sup> )	TEAC <sup>D</sup> (Trolox eq μM L <sup>-1</sup> )
OSB1	2.54 a	0.619 de	4.10	4.24 × 10 <sup>-17</sup> a	5.65 e
OSB2	2.26 bc	1.131 b	2.00	1.92 × 10 <sup>-17</sup> b	16.99 a
OSB3	2.13 c	0.594 e	3.59	4.48 × 10 <sup>-17</sup> a	3.69 f
OSB4	2.48 a	1.156 b	2.15	1.85 × 10 <sup>-17</sup> b	13.08 c
OLG1	2.38 ab	0.753 c	3.16	4.21 × 10 <sup>-17</sup> a	15.81 b
OLG2	1.70 d	0.684 d	2.49	1.18 × 10 <sup>-17</sup> c	4.06 f
ELG	1.61 d	1.451 a	1.11	1.84 × 10 <sup>-17</sup> b	10.14 d

<sup>A</sup>Means within columns followed by the same letter are not significantly different using Tukey's test ( $\alpha = 0.05$ ). Triplicate analyses were conducted for each parameter except the EAC/EDC ratio that was determined by dividing the mean value for EAC by the mean value of the EDC for each HA.

<sup>B</sup>HA EAC and EDC were determined using purified HAs via mediated electrochemical reduction and oxidation, respectively, as described in Aeschbacher et al. (2010).

<sup>C</sup>Semiquinone free radical concentrations (SFRC) were determined using purified HAs dissolved in 0.1 N NaOH on an Active Spectrum MicroESR spectrometer operating at X-band frequencies.

<sup>D</sup>Trolox equivalent antioxidant capacity (TEAC) was determined on purified HAs using the assay described by Re et al. (1999) and modified by Mingle and Newsome (2020).

**TABLE 8** |  $^{13}\text{C}$ -NMR results from the distribution of %C in the various assigned chemical shift region area integrations.

HA Sample	-----%C-----										
	Ali.	Complex. Ali.	Methoxyl	O-Alkyl	Anom.	Aro I.	Aro II.	Phe.	Carbox.	Ketonic	HB <sup>A</sup>
	------(ppm)-----										
	(0–35)	(35–50)	(50–60)	(60–96)	(96–108)	(108–120)	(120–145)	(145–162)	(162–190)	(190–216)	
OSB1	16.7	7.4	2.9	9.2	5.2	10.6	31.5	8.4	7.7	0.4	2.94
OSB2	16.3	9.0	3.9	8.8	4.2	9.3	25.2	10.2	10.6	2.6	2.33
OSB3	14.9	6.6	2.7	6.1	5.2	10.5	32.6	9.9	9.5	2.0	2.92
OSB4	15.8	9.3	4.1	8.0	6.5	11.6	26.8	9.0	7.7	1.2	2.64
OLG1	15.7	6.9	1.8	3.3	3.8	9.9	36.4	10.4	9.8	2.0	3.80
OLG2	22.5	8.0	5.4	6.0	3.7	8.6	28.2	7.8	8.8	0.9	3.03
ELG	19.6	8.7	3.8	8.4	7.0	10.3	22.8	10.0	8.2	1.2	2.50

<sup>A</sup>Hydrophobic Index (HB) = ratio of hydrophobic C/hydrophilic C:  $HB = [(0-50) + (108-162)] / [(50-108) + (162-216)]$  (after Dobbss et al., 2010 with slight modifications in chemical shift regions).

### $^{13}\text{C}$ -NMR Analysis

The results of the  $^{13}\text{C}$ -NMR spectral distribution for the HAs is given in **Table 8** and the  $^{13}\text{C}$ -NMR spectra are shown in **Supplementary Figure 4**. To identify and simplify the differences among their carbon distribution, the data in **Table 7** were subjected to principal component analysis (PCA). **Table 8** summarizes the regions of the chemical shift most correlated to each humic product for PC1 and PC2 (explaining 68.15% of total variance) and PC1 and PC3 (explaining 57.37% of total variance). The C in the OSB1 and OSB4 HAs was distributed among aromatic I, anomeric, and O-Alkyl C. The relative distribution of C in OSB3 was associated with the aromatic II and phenolic regions, whereas OLG1 was comparatively enriched in aromatic II C with a larger ketone C content. Compared to the other HAs, the OSB2 HA showed a mix of aromatic II and aliphatic C with a strong presence of carboxyl C, while in OLG2 a major aliphatic and methoxyl C distribution was observed. The ELG HA C was comparatively less aromatic, with a strong complex aliphatic component and a moderate presence of O-Alkyl C.

### Molecular Mixing Model

The application of the molecular mixing model elucidated additional trends in the data by gathering the  $^{13}\text{C}$  NMR assignments into organic biomolecule classes (**Figure 1**). As expected, the ELG HA, which was obtained from the geologically youngest ore source, had the lowest CAS and highest lignin content (**Figure 1**). The largest differences among the chemical groups occurred in CAS and lignin contents. As the process of coalification proceeds, the concentrations of lignin-related molecules decrease with a concomitant increase in CAS formation due to cross-linking of aromatic rings leading to condensation of lignin-derived structures (Hatcher et al., 1990). Therefore, it is interesting that the OLG1 HA had a greater amount of CAS and lower amount of lignin than the OSB-derived HA, with the exception of the lignin content of the OSB1 HA. However, as previously stated, the ores are all oxidized forms of the original coal and thus had varied conditions and times of oxidative exposure. Also of note, the three HAs with

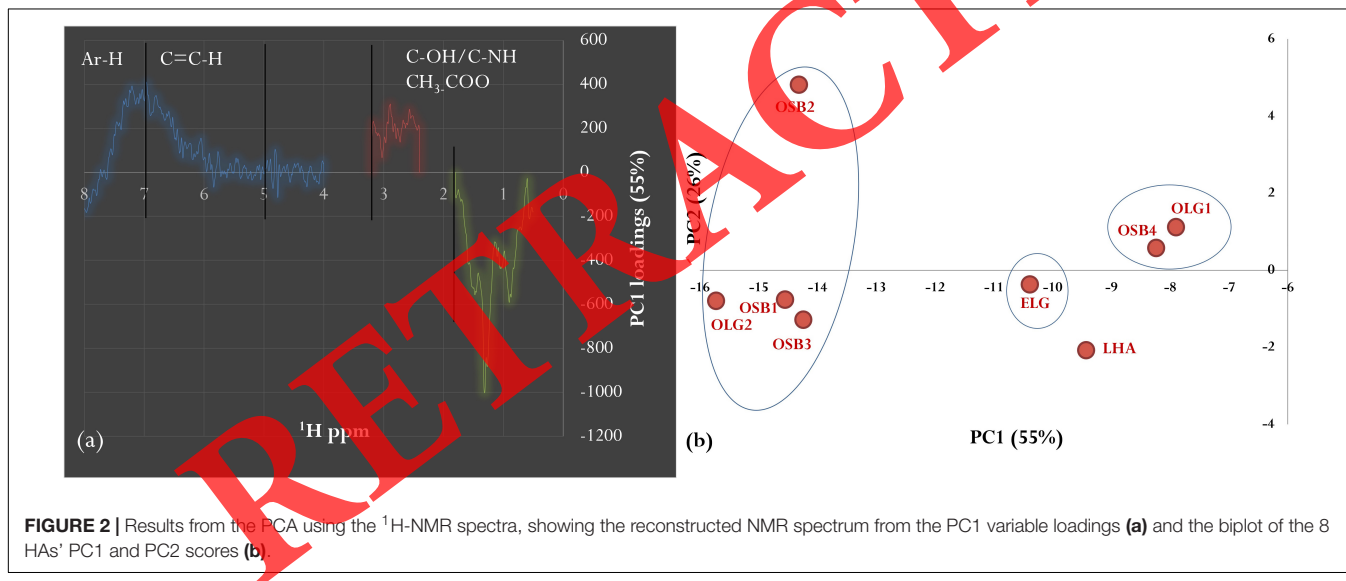
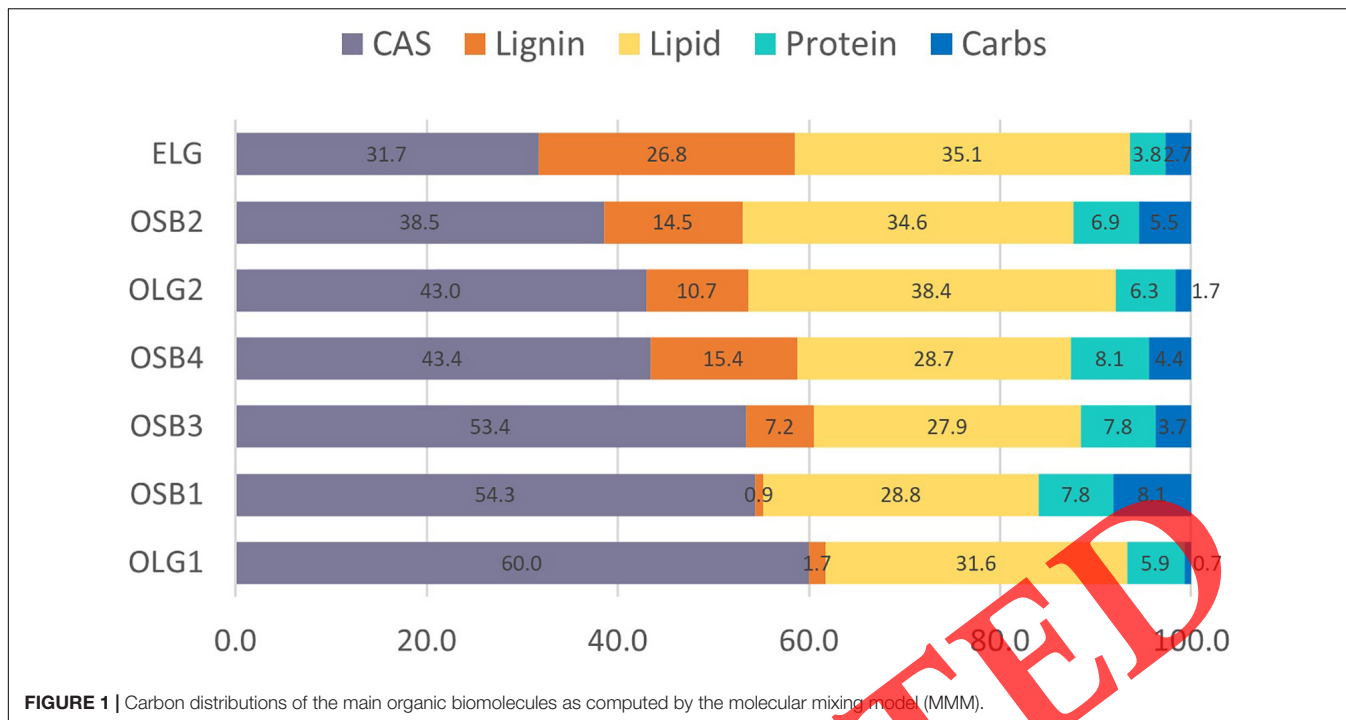
the highest CAS content also had the highest EAC/EDC and SFRC (**Table 6**).

### $^1\text{H}$ -NMR Results

The  $^1\text{H}$ -NMR spectra for the seven purified HAs and the IHSS leonardite HA are shown in **Supplementary Figures 5–8**. The peak areas were integrated, and their resulting areas are shown in the supporting information **Supplementary Table 2**. The 7 ore HAs contained varying areas in the aliphatic (0.5–1.8 ppm chemical shift), oxygenated (2.1–5 ppm chemical shift), olefin (5–7 ppm), and aromatic (7–9 ppm) regions. To assist with understanding the compositional differences amongst the ore HAs [including the leonardite humic acid (IHSS LHS) standard], principal component analysis (PCA) was conducted utilizing the spectral intensities at every 0.004 ppm (as described in the methods section). **Figure 2a** shows the reconstructed NMR spectra from the PC1 variable loadings, with the samples scores shown in **Figure 2b**. PC1 explained 55% of the variance of the 1535 variables among the 8 HAs, while PC2 explained an additional 26% of the variance (total 81% of variance explained by PC1 and PC2). Thus, the horizontal spacing is more important in **Figure 2** than the vertical. It is apparent from the PC1 spectrum that the most important features were the olefin/aromatic region at 6–8 ppm, the oxygenated region at 2.4–3 ppm, and the aliphatic region at 0.5–1.8 ppm. Samples with high negative scores (OSB1, OSB2, OSB3, and OLG2) are more enriched in the aliphatic region, while samples with low negative PC1 scores (OLG1, OSB4, ELG, and LHA) are comparatively more enriched in the oxygenated and aromatic regions. Overall, when going from left to right in **Figure 2b**, the HAs become more aromatic.

### Fourier Transform Ion Cyclotron Resonance Mass Spectrometry Analysis

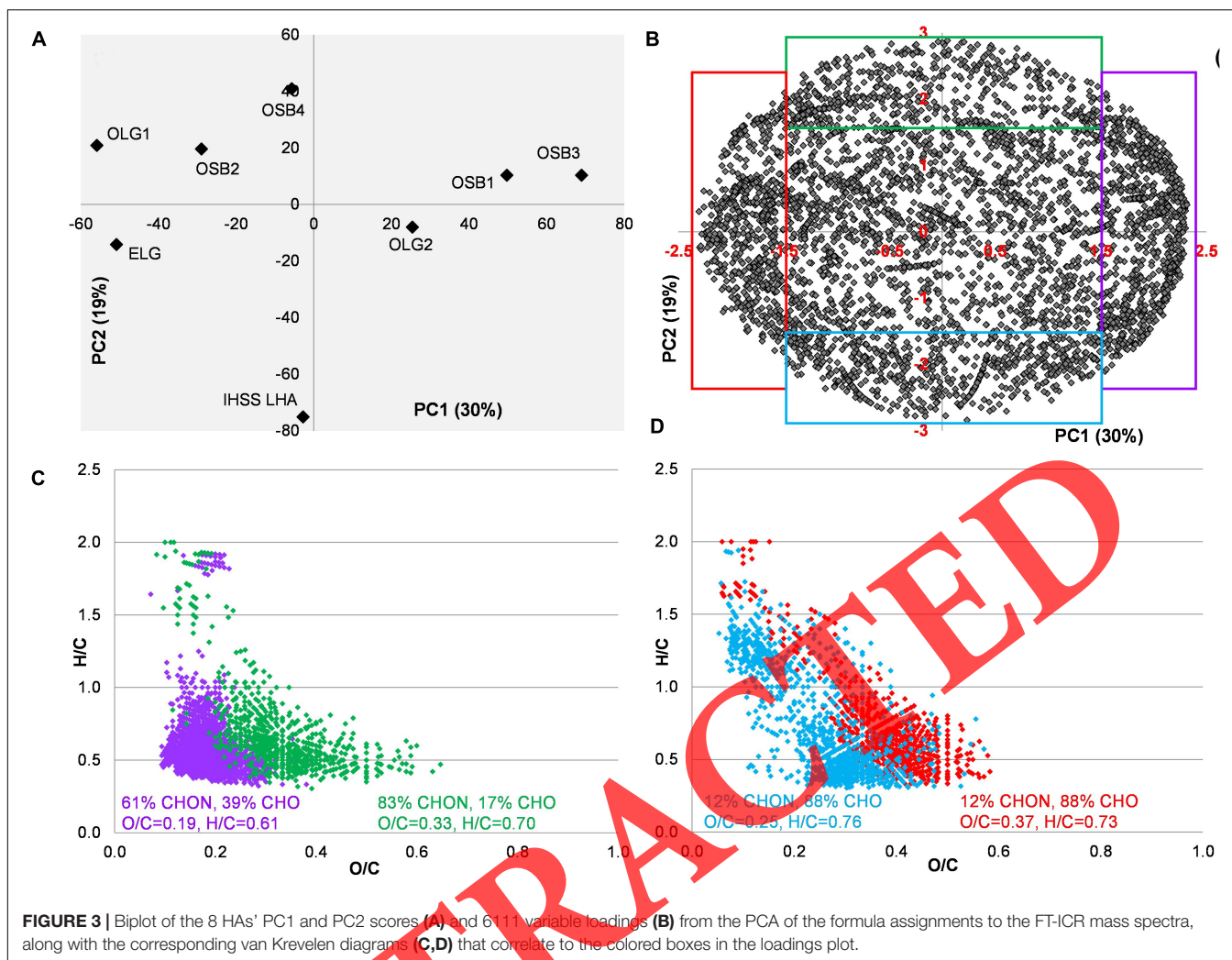
As shown in **Supplementary Table 3** in the supporting information, the ore HAs and IHSS leonardite HA have number-averaged O/C and H/C ratios in the range of 0.24 to 0.30 and 0.72 to 0.86, respectively. The ore HAs also have very few S-containing formulas, which is consistent with the elemental



composition shown in **Table 4**, but have a significant contribution from N-containing formulas (**Supplementary Table 4** in the supporting information). Over 99% of the total spectral magnitude in the ore samples is accounted for by CHO and CHON formulas. Individual van Krevelen diagrams (Kim et al., 2003) are also shown in the supporting information (**Supplementary Figures 9–12**) and based on the alignment of the formulas in van Krevelen space and the modified aromaticity index (Koch and Dittmar, 2006, 2016), a biomolecular compound class can be assigned (Hockaday et al., 2009; Ohno et al., 2010). For the ore HAs, most formulas align in the region associated with condensed aromatics, with some falling into the lower O/C

region of the lignin-like space in the center of the van Krevelen diagram (**Supplementary Table 5**).

Principal component analysis was also conducted on the formulas assigned to these samples, as described in the methods section. **Figure 3** shows the biplot of the scores of the samples and the loadings of the variables where PC1 explains 30% of the variance of the 6,111 variables among the eight samples, and PC2 explains another 19%. Areas containing variable loadings (i.e., formulas) and scores (i.e., samples) in the same quadrant indicate a close correspondence of formulas with high relative magnitudes being detected in those specific samples. Loadings that are far from the origin are those that impact the variance of the samples



the most. OSB2, OSB4, OLG1, ELG, and LHA have negative PC1 scores (Figure 3A) and are thus enriched in formulas that fall in the red box (Figure 3B). OSB1, OSB3, and OLG2 have positive PC1 scores and are enriched in the formulas that fall in the purple box of the loadings plot. OSB4 has a high positive PC2 score (enriched in formulas in the green box), while LHA has a high negative PC2 score (enriched in formulas in the blue box). The formulas are color-coded and plotted on the corresponding van Krevelen diagrams, as shown in Figures 3C,D.

Of the 6111 formulas, 1127 (18%) had high PC1 loadings, falling into the purple box of Figure 3B. These formulas in purple (enriched in OSB1, OSB3, and OLG2) mostly have very low O/C ratios (<0.3), low H/C ratios (<1), consist of 61% N-containing and 39% CHO-only, and have average O/C and H/C ratios of 0.19 and 0.61, respectively. About 11% of the formulas (661 of 6,111) fall into the red box. These formulas (12% N-containing and 88% CHO-only) are primarily enriched in OSB2, OLG1, and ELG, and while these formulas also mostly have low H/C ratios, they have higher O/C ratios (0.3–0.6) than the purple group (average O/C and H/C ratios of 0.37 and 0.73, respectively). This is consistent with the  $^1\text{H-NMR}$  data that showed OLG1, OSB4,

and ELG were more oxygenated. The formulas in green (651 of 6111, 11%) that are enriched in OSB4 are 83% N-containing (average O/C and H/C ratios of 0.33 and 0.70, respectively). OSB1, OSB3, and OSB4 have the highest %N values (Table 4), which is consistent with the PCA here that shows enrichment specifically in these groups of CHON-containing formulas. The blue formulas (903 of 6111, 15%) are enriched in LHA and are 88% CHO-only (average O/C and H/C ratios of 0.25 and 0.76, respectively).

### Fourier Transform Infrared Spectra

The FTIR spectra of the seven purified ore-derived HAs are shown in Supplementary Figure 13. Infrared absorptions were assigned to functional groups and classes of compounds based on assignments reported previously (Lambert, 1987; Piccolo et al., 1992b; Smith, 1999; Tatzber et al., 2007). The spectra from the seven ore-based HAs were characterized by the following major bands: a very broad band at  $3,420\text{--}3,250\text{ cm}^{-1}$  (H-bonded primarily OH stretch but also NH groups); a very broad band at  $3,100\text{--}2,400\text{ cm}^{-1}$  (H-bonded OH stretch in carboxylic acids); a slight shoulder at  $3,067\text{--}3,074\text{ cm}^{-1}$  (aromatic C-H stretching);

a sharp peak at 2,915–2,923  $\text{cm}^{-1}$  and a peak or shoulder at 2,845–2,852  $\text{cm}^{-1}$  (respectively, asymmetric and symmetric C-H stretch of  $\text{CH}_2$  aliphatics); a strong peak at 1,701–1,706  $\text{cm}^{-1}$  (aromatic C = O stretch of carboxylic acids); a strong peak at 1,598–1,603  $\text{cm}^{-1}$  (asymmetric  $\text{COO}^-$  stretch of carboxylates); a smaller peak at 1,418–1,428  $\text{cm}^{-1}$  (symmetric  $\text{COO}^-$  stretch of carboxylates); a smaller peak at 1,373–1,379  $\text{cm}^{-1}$  (could be a second symmetric  $\text{COO}^-$  stretch of carboxylates); a strong peak at 1,197–1,217  $\text{cm}^{-1}$  (C-O stretch of phenols) with the exception of the OLG3 that has a peak at 1,172  $\text{cm}^{-1}$  (C-O stretch of 2° alcohols); and a small peak at 761–768  $\text{cm}^{-1}$  (ortho-substituted aromatic out-of-plane C-H bending).

Unfortunately, the ATR-FTIR analysis does not provide quantitative data like the  $^{13}\text{C}$ -NMR analysis. However, the relative abundance of a particular chemical entity can be compared among the FTIR spectra. For example, the peaks in the vicinity of 2,920 and 2,850  $\text{cm}^{-1}$  are due to aliphatic C. These peaks in the OLG1 and OSB4 HA spectra are not as pronounced or distinct as they are in the spectra of the other HAs. These are the two HA that had the least aliphatic protons in the  $^1\text{H}$ -NMR analysis (Figure 2) and their C was not associated with aliphaticity in the  $^{13}\text{C}$ -NMR analysis (Table 4 and Figure 1). Thus, the FTIR does confirm the less aliphatic nature of the OSB4 and OLG1 HAs.

The difference spectrum of the average of the resolution enhanced OSB1/OSB3/OLG1 (i.e., TRL-F<sup>++</sup>) spectra and the average of the resolution enhanced OSB2/OSB4/ELG (i.e., TRL-F) spectra is shown in Figure 4A. This spectrum was then used to prepare the spectrum that illustrates the peaks that predominated in the TRL-F<sup>++</sup> HAs (Figure 4B) and the spectrum that illustrates the predominant peaks in TRL-F HAs (Figure 4C). Interestingly, two of the most prominent peaks in the TRL-F<sup>++</sup> spectrum (Figure 4B) found at 1,228 and 1,711  $\text{cm}^{-1}$  have been assigned to asymmetric  $\text{PO}_2^-$  and C = O stretching in flavin adenine dinucleotide (FAD) (Spexard et al., 2011). While FAD is highly oxidative, it has never, to the authors knowledge, been found in HA. However, the peak at 1,711  $\text{cm}^{-1}$  has also been assigned to C = O stretching in thymoquinone (Rani et al., 2018) and the peak at 1590  $\text{cm}^{-1}$  has been assigned to C = C stretching of the unsaturated part of the quinone ring (Bandaranayake et al., 2006). The interpretation of the presence of quinones would be more consistent with the higher SFRC and EAC possessed by TRL-F<sup>++</sup> HAs compared to the TRL-F HAs (Table 6). The peak pattern of the TRL-F HAs (Figure 4C) was very similar to that of a cross-linked chalcone that had stretching bands of the C = O ester, and  $\alpha$ ,  $\beta$ -unsaturated C = O were observed at 1,722 and 1,606  $\text{cm}^{-1}$ , respectively (Ramagathan et al., 2015). In addition, the peak at 1,508  $\text{cm}^{-1}$  was attributed to the stretching mode of the aromatic C = C group. Similarly, in the TRL-F spectrum the 1,734  $\text{cm}^{-1}$  and the 1,619 and 1,576  $\text{cm}^{-1}$  peaks could be assigned to C = O ester and  $\alpha$ , $\beta$ -unsaturated C = O, respectively. In addition, the peak at 1156  $\text{cm}^{-1}$  can be assigned to C-O-C stretching of glycosidic linkages (Sinyayev et al., 2020). The presence in the TRL-F HAs of glycosylated polyphenols, which have significant antioxidant potential (Xiao et al., 2021), is consistent with the strong

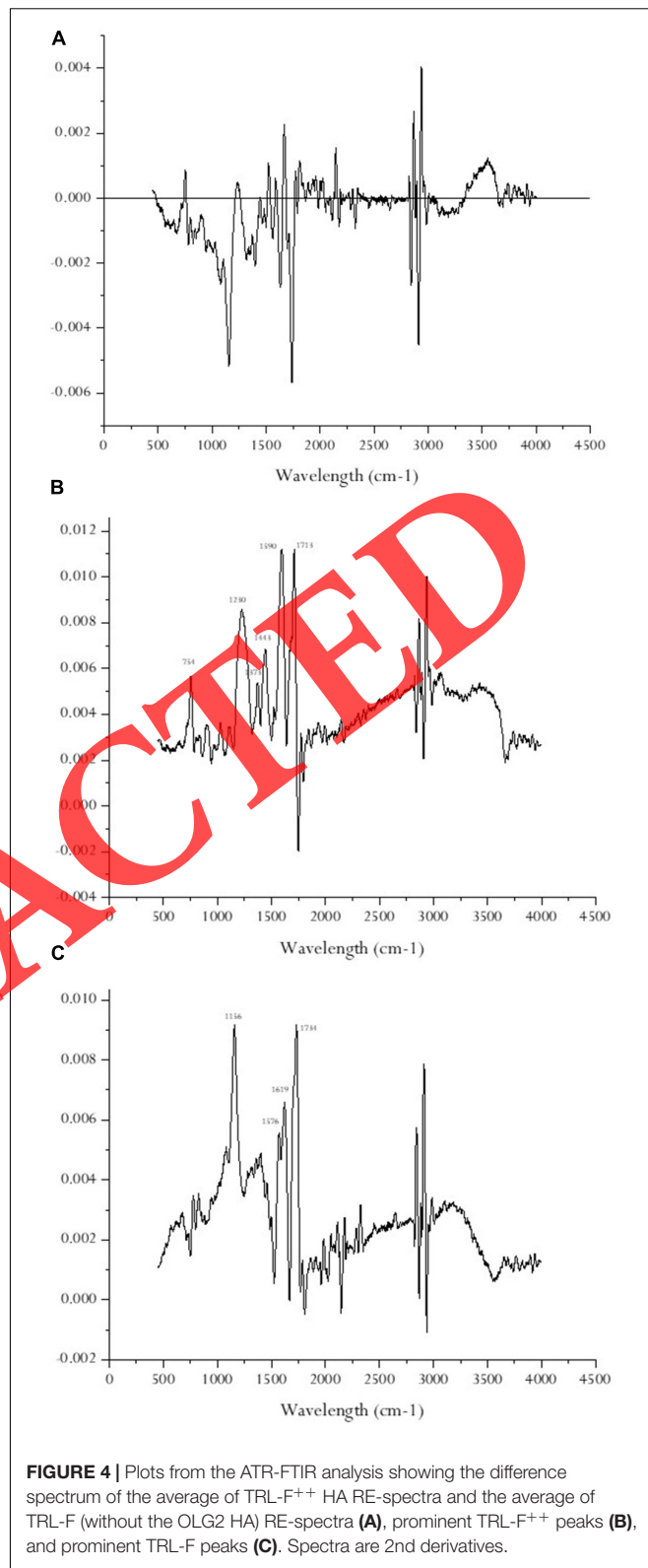
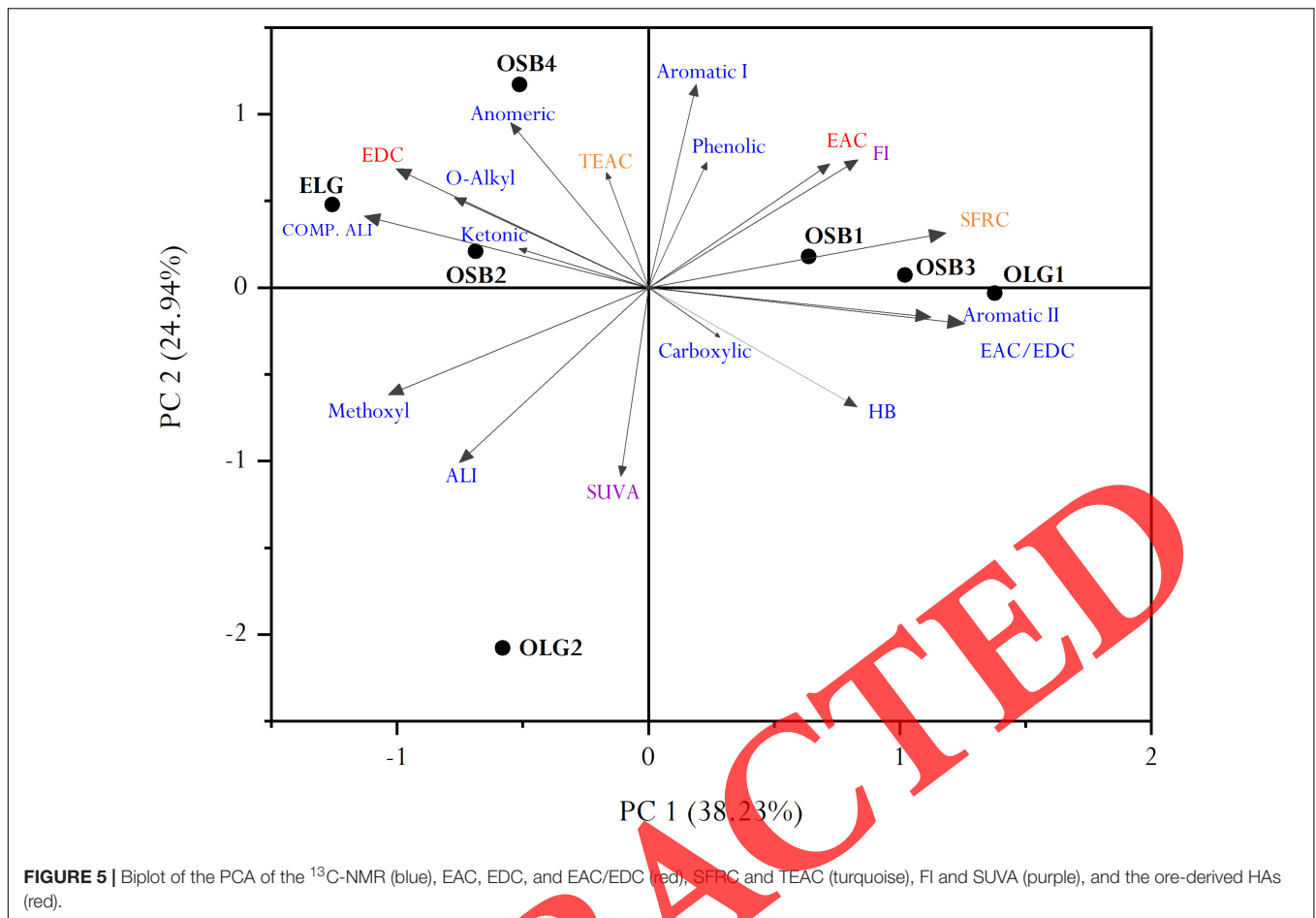


**FIGURE 4** | Plots from the ATR-FTIR analysis showing the difference spectrum of the average of TRL-F<sup>++</sup> HA RE-spectra and the average of TRL-F (without the OLG2 HA) RE-spectra (A), prominent TRL-F<sup>++</sup> peaks (B), and prominent TRL-F peaks (C). Spectra are 2nd derivatives.

correlation of these HAs with O-alkyl and anomeric type C, EDC (Figure 5), and the fact that these HAs had the highest TEAC values (Table 6).



## Maize Bioassay

Application of all HA to corn seedlings at 8 mM C L<sup>-1</sup> resulted in positive but variable increases in plant morphological parameters compared with controls (Table 5). The variable effects resulted in the production of corn seedlings with racially different phenotypes from overall larger seedlings produced by treatment with the OSB3 and OSB4 HAs to seedlings with smaller shoots and roots but more highly ramified root systems as were produced by treatment with the OSB1 HA.

Treatment with OSB3 and OSB4 HA resulted in the greatest increases in total dry weight (TDW) but the increases were only significantly greater than increases produced by treatment with OSB2 and OLG2 HAs. The greatest increase in shoot dry weight (SDW) was produced by the OSB4 HA. The increase produced by this HA was significantly greater than increases produced by all other HAs except the OSB2 HA. The greatest increases in leaf length (LL) and leaf surface area (LSA) were produced by application of OSB3 and OSB4 HAs. Percent increases in LL and LSA produced by the OLG1 HA were minor compared to the other HAs. Increases in root dry weight (RDW) were far greater in seedlings treated with the OSB3, OSB4, and OLG2 HAs than for the remaining HAs that produced significantly smaller increases. Despite having the second smallest increase in RDW, the greatest increase in total root length (TRL) was produced by

treatment with the OSB1 HA. However, this is consistent with this HA also producing the greatest increase, by far, in TRL in the 0–0.5 mm diameter class. Interestingly, the OSB3 HA produced one of the highest RDW increases accompanied by the second greatest increase in TRL, which included significant increases in all three root diameter classes. This also resulted in one of the greatest increases in root surface area (RSA).

The total percentage increase score (TPS) is a summation of the percent increases for all the biomass and morphological parameters and provides a comparison of the overall effect of the various HAs on seedling growth. Based on the TPS, the OSB3 and OSB4 HAs had the greatest impact on corn seedling growth compared to the control plants. The HA that had the least effect on plant growth were the ELG and OLG1 HAs.

## Principal Component Analysis of Humic Acids Analytical Data

In PCA1, the first two PCs explained 63.17% of the variance, with PC1 and PC2 accounting for 38.23 and 24.94% of the variation, respectively (Figure 5). Based on variable loadings, PC1 separated samples based on aromaticity and parameters associated with it, such as HB, EAC, EAC/EDC, SFRC, and FI all having positive PC1 loading values. Aliphaticity, methoxyl, O-alkyl, anomeric, and ketonic functionalities (as determined by

$^{13}\text{C}$ -NMR) and EDC and TEAC had negative PC1 loading values. Variables impacting the variance along PC2 were anomeric, aromatic I, and perhaps, to a lesser extent, EAC and FI, all having positive PC2 loadings. The important variables having negative PC2 loadings were aliphatic, SUVA, and HB. Based on the measured chemical parameters, the HAs could be separated as follows based on the PCA biplot (Figure 5). The OSB1, OSB3, and OLG1 HAs were strongly associated with aromatic II, SFRC and EAC, EAC/EDC, FI, and HB. This is consistent with the aromatic nature of quinones that provide both SFRC and EAC and the fact that, to a large extent, fluorescence in NOM resides in quinones (Cory and McKnight, 2005). The OLG2 HA was associated with aliphatic C and methoxyl functionality. Interestingly, this HA was also associated with  $\text{SUVA}_{254}$ , which is generally thought to be an indicator of aromaticity (Weishaar et al., 2003). In this case, however, it is more associated with aliphaticity as determined by  $^{13}\text{C}$ -NMR. The OSB2 and ELG HAs were associated with aliphaticity, EDC, and ketonic and O-alkyl functionalities. Finally, the OSB4 HA was associated with anomeric type C and TEAC (i.e., antioxidant activity). Oligosaccharides, which contain anomeric C, possess significant antioxidant activities (Hou et al., 2015; Wang et al., 2016; Devi et al., 2019).

## Principal Component Analysis of Humic Acid Analytical Data and Corn Seedling Biomass and Root and Shoot Morphological Parameters

In PCA2, the HA analytical data analyzed in PCA1 were combined with the corn seedling root and shoot biomass and morphological data to determine which chemistries were driving the plant biostimulant response (PBR). The first three PCs accounted for 76.00% of the variance, with PC1, PC2, and PC3 accounting for 28.93, 28.05, and 19.02% of the variance, respectively (Figure 6). In the PC1/PC2 biplot, PC1 separated the HAs into two groups (Figure 6A). The first group, with negative PC1 scores, included OSB1, OSB3, and OLG1. These HAs were associated with aromatic II, SFRC, and therefore pro-oxidant activity, and other parameters associated with quinones including EAC, EAC/EDC ratio, and FI. These HAs were also strongly associated with promoting fine root growth (i.e., TRL-F) and because of the magnitude of TRL-F stimulation, overall TRL. PC1 HAs with positive scores included OSB2, OSB4, OLG2, and ELG (Figure 6A). These HAs were associated with aliphatic and anomeric type C and ketonic, O-alkyl, and methoxyl functionalities. They were also associated with EDC and TEAC, both of which indicate relatively higher antioxidant activity.

The biplot of PC1/PC3 (Figure 6B) illustrates the strong relationships between fine root growth (i.e., TRL-F) and the EAC/EDC ratio and that the EAC, from semiquinone-type free radicals, was associated with aromatic II type C. The OSB1, OSB3, and OLG1 HAs were strongly associated with SFRC, aromatic II type C, EAC, EAC/EDC, and interestingly, HB. HB has been shown to be correlated with various measurements of root system stimulation in previous SAR studies (Canellas et al., 2009, 2012;

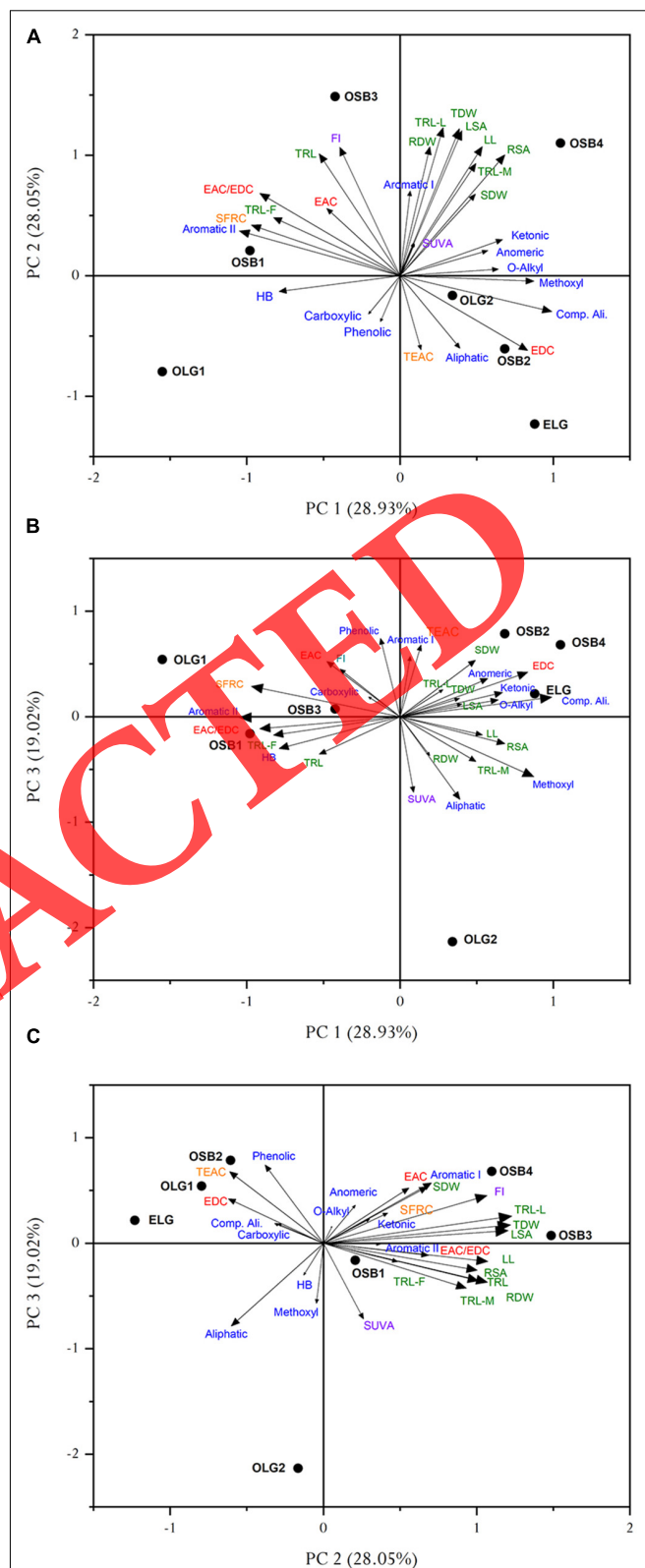


**FIGURE 6** | PC2 biplots of HA analytical parameters and corn seedling biomass and root and shoot morphological parameters. (A) PC1/PC2 biplot. (B) PC1/PC3 biplot. (C) PC2/PC3 biplot.

Dobbss et al., 2010). The association of HB with root growth stimulation could be because semiquinone-type free radicals are contained in the HB HA fraction. The PC1/PC3 biplot also demonstrates the close association of OSB2 and OSB4 HAs with carbohydrate type C (i.e., anomeric and O-alkyl) and with EDC and TEAC, which demonstrated strong antioxidant activity for these HAs. Carbohydrates have been shown to possess significant antioxidant potential (Hou et al., 2015; Wang et al., 2016; Devi et al., 2019). The OSB4 HA stimulated overall corn seedling growth to the second greatest extent, slightly less than OSB3 HA (Table 5). The close association of OSB3 with pro-oxidant-related parameters (including SFRC and EAC/EDC) and the OSB4 HA with strong associations with antioxidant-related parameters including EDC and TEAC suggest that redox activity may play an important role in the HA PBR.

In the PC2/PC3 biplot, the HAs that had the most impact on corn seedling growth (i.e., OSB3 and OSB4) and on fine root growth (i.e., OSB1) are grouped together with positive PC2 scores (Figure 6C). These HAs were, again, associated with aromaticity, SFRC, EAC, EAC/EDC, FI, and all of the plant biomass and shoot and root morphological parameters. HAs with negative PC2 loadings included OSB2, OLG1, OLG2, and ELG. These HAs were associated with aliphaticity, phenolic, carboxylic, and methoxyl functionalities and antioxidant activity-related parameters such as EDC and TEAC. Strong association of SFRC and related parameters with strong relative stimulation of corn seedling growth suggests again, that pro-oxidant activity is important to HA biostimulation. The fact that EAC/EDC was consistently associated with strong plant response also suggests that the ratio of pro-oxidant to antioxidant activity plays an important role in mediating the HA PBR.

## DISCUSSION

The expanding use of HS in the agricultural and horticultural sectors substantiates the claims of their effectiveness as crop plant biostimulants, which can help these industries respond to the ever-increasing demands for food production in the face of increases in the frequency of abiotic stresses imposed by climate change. There is, however, ample room for improvement to HS product effectiveness and performance consistency. Some improvements in these areas can be made through gaining more experience in fine-tuning rates and timings of applications tailored to specific crops. Improvements can also be made through identifying the HS chemistries that are responsible for elicitation of the PBR, elucidating the relationship between the concentrations of these chemistries and the magnitude of the plant stress response that results in an optimized PBR and using this information to tailor products for specific applications. The chemical complexity of HS has made identification of specific PBR elicitors extremely difficult.

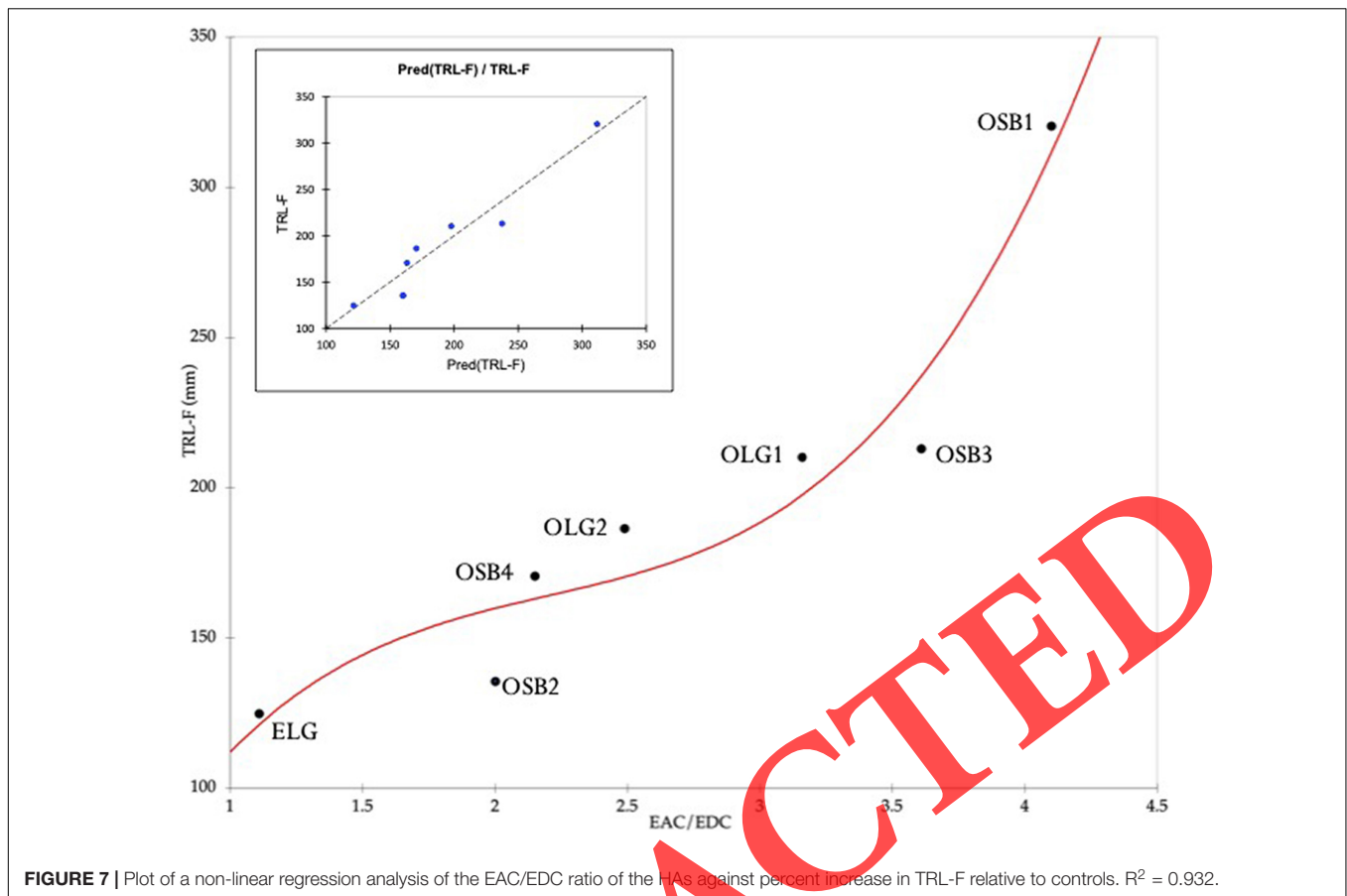
In the present investigation, the effects of seven extensively chemically characterized, ore-derived HAs on biomass accumulation and root and shoot morphologies of corn seedlings grown in minimal liquid medium, during the first week of growth, was examined. At a rate of 8 mM C L<sup>-1</sup>, all

seven HAs produced increases in corn seedling biomass and root and shoot morphological parameters, relative to control seedlings, that varied significantly among the HA treatments (Table 5). The HAs were added to the liquid medium, so this study examined HA root application, which is typically how HS are applied in commercial AG. No nutrients were added to the liquid medium, so the growth of the seedlings was entirely reliant on nutrients stored in the seeds. Thus, the significant differences observed among the HA treatments in corn seedling root and shoot biomass and morphology were a direct result of differences in chemistries among the seven HAs.

The HAs were all obtained from geographically distinct brown coal (ELG), oxidized lignite (OLG1, OLG2), or oxidized sub-bituminous (OSB) coals, all of which are used as sources for the production of commercial HS products. The HAs obtained from the ores varied significantly in their chemistries, particularly in degrees of aromaticity versus aliphaticity, but also in SFRC, EAC, EDC, EAC/EDC ratio, and antioxidant contents (i.e., TEAC values), all of which had significant effects on producing biomass accumulation and morphological differences among the HA treatments.

The most salient SAR finding of this study was the strong association of SFRC and promotion of fine root (i.e., TRL-F 0–0.5 diameter) growth that was revealed in PCA2 (Section “Principal Component Analysis of Humic Acid Analytical Data and Corn Seedling Biomass and Root and Shoot Morphological Parameters,” Figures 6A–C). The strong correlation of SFRC and lateral root growth promotion is consistent with the findings of Canellas et al. (2008), who also reported a strong positive Pearson correlation (i.e., 0.82,  $p \leq 0.05$ ) between SFRC and root area, the latter of which is also a measure of lateral root growth (Grover et al., 2021). The three HAs, OSB1, OSB3, and OLG1 that promoted TRL-F to the greatest extents relative to controls (Table 5) also had the highest SFRC (Table 6). However, the higher SFRC does not explain greater fine root growth completely. In all three of the PCA2 biplots (Figures 6A–C), TRL-F was most closely associated with the EAC/EDC ratio. In fact, a non-linear regression analysis of the EAC/EDC ratio against the percent increase in the TRL-F (Figure 7) revealed a strong positive relationship ( $R^2 = 0.932$ ) between the two parameters, suggesting that it is the ratio of the pro-oxidant EAC (which originates primarily in the SFRC) and the antioxidant EDC (which typically originates in the phenolic fraction) that is important to the stimulation of fine root production.

Plants respond to abiotic stresses through both physiological and morphological responses (Yadav et al., 2020). Many of these same responses, for example, physiological responses like increases in  $[Ca^{2+}]_{cyt}$  (Ramos et al., 2015), increased production of antioxidants (Moghadam et al., 2014; Hemida et al., 2017), and morphological changes to root system architecture (Canellas et al., 2008, 2009, 2010; Bobik et al., 2010; Canellas et al., 2012; Aguiar et al., 2009, 2013; Dobbss et al., 2010; Muscolo et al., 2010; David et al., 2014; Garcia et al., 2016; van Tol de Castro et al., 2021) have also been observed in plants treated with HS. Plants exposed to abiotic stress typically develop recognizable morphological changes, called stress-induced morphogenesis responses (SIMS), to root systems that include re-differentiation



of the pericycle and formation of lateral roots, inhibition of root cell elongation, formation of root hairs in the apex, and blocked cell division in the primary meristem (Patakas, 2011). In many reports, application of HA has resulted in increases in numbers of lateral roots, lateral root length, and density (Aguiar et al., 2009; Canellas et al., 2009, 2010, 2011, 2012; Dobbss et al., 2010; Muscolo et al., 2010; Aguiar et al., 2013; David et al., 2014; Garcia et al., 2016; van Tol de Castro et al., 2021). However, in some cases, increases in lateral roots have been accompanied by increases in the principal root length (Aguiar et al., 2009; Canellas et al., 2009; van Tol de Castro et al., 2021), root diameter (Aguiar et al., 2013; Garcia et al., 2016), or both (Canellas et al., 2010). Therefore, although in most cases while exposure of plants to HAs does result in increased root system ramification, HAs have also caused increases in primary root length, which does not conform to the typical SIMS.

A comparison of the HA-induced TRL-F morphologies along the EAC/EDC continuum shown in **Figure 7** may offer a possible explanation for the reported HA-induced root morphological differences. The EAC/EDC ratio represents the ratio of pro-oxidant and antioxidant capacities of the HAs. As pro-oxidants, quinones can accept electrons, for example, from PM NAD(P)H oxidases and then reduce molecular oxygen to the superoxide radical (Van Gestelen et al., 1998). This can lead to further ROS formation [i.e.,  $H_2O_2$  and hydroxyl radical (HO.)] and initiate

and extend the stress response. As antioxidants, polyphenols in HAs can scavenge ROS, reduce their signaling and tissue damaging effects, and thus attenuate the stress response (Ueda et al., 2004). In the present investigation, the HA with the highest EAC/EDC ratio (i.e., 4.1), OSB1, produced plants with the typical SIMS response with reduced overall plant growth but a highly ramified fine root system (**Table 5**). The HA with the second highest EAC/EDC, OSB3, also produced plants with more highly ramified fine root systems but larger root systems and plants, in general. The EAC of the OSB3 HA was significantly less than that of the OSB1 HA. Therefore, even though the OSB3 HA EAC/EDC was the second highest, the overall pro-oxidant activity was less than in the OSB1 HA. Therefore, in addition to the EAC/EDC ratio, the magnitude of the EAC or pro-oxidant and the intensity of the resulting stress response produced, might also play a role. This is consistent with the magnitude of the stress response being highly dependent on the concentration and extent of the stress elicitor (Qudeimat and Frank, 2009). Treatment with the OLG1 HA had a similar effect on plant morphology compared to OSB1, including a more highly ramified root system. However, the effect was not as great in keeping with a relatively lower EAC (**Table 6**). The OLG2 and ELG HAs had the lowest EACs. While the OLG2 HA still stimulated fine root growth with an EAC/EDC value of 2.49, the ELG HA with the significantly largest EDC, and an EAC/EDC ratio of 1.11 had very little effect on corn seedling

growth, maybe due to the balanced pro-oxidant/antioxidant ratio. The OSB2 and OSB4 HAs had similar values for EAC/EDC of 2.0 and 2.15, respectively. However, the OSB4 HA produced a significantly larger corn seedling (Table 5). The OSB4 HA was just as efficient in promoting corn seedling growth as the OSB3 HA and like the OSB3 HA, promoted both root and shoot growth (Table 5). OSB4 HA was strongly associated with anomeric and O-alkyl C and EDC (Figure 6B), but was also associated with aromaticity based on the  $^1\text{H-NMR}$  PCA (Figure 2b). That the EDC and TEAC were strongly associated with anomeric C and O-alkyl C (Figure 6) was interesting and unexpected, simply because phenols are generally thought to be the primary source of EDC. However, in nature, glycosylated structures, e.g., polyphenolic glycosides (e.g., quercitrin), are typical, rather than the exception (Lindroth and Pajutee, 1987). A glycoside is any molecule in which a sugar group is bonded through its anomeric carbon to another group via a glycosidic bond. The anomeric C in a 6-C sugar is the C attached to the O that is not attached to a  $\text{CH}_2\text{OH}$  group. Glycosides can be linked by an O- (an O-glycoside), N- (a glycosylamine), S- (a thioglycoside), or C- (a C-glycoside) glycosidic bond. Phenolic glycosides are O-glycosides. The sugar group is known as the glycone and the non-sugar group as the aglycone or genin part of the glycoside. The glycone can consist of a single sugar group (monosaccharide) or several sugar groups (oligosaccharides). Plants produce a number of different glycosides (e.g., anthocyanins), which are glycosides of anthocyanidins (i.e., anthocyanidins with a sugar attached). Evidence for the existence of these types of structures in HAs comes from the release of sugars during hydrolysis of HAs (Hayes, 1984) and direct evidence from selective methylations that demonstrated the existence of carbohydrate hydroxyl groups (Wershaw et al., 1981). Different types of phenolics are the most abundant secondary metabolites in plants, and plant polyphenols are drawing increasing attention due to their antioxidant properties, i.e., the ability to donate electrons (Dai and Munper, 2010). Plant polyphenolic glycosides also possess antioxidant activity, but they are not as active as their aglycones and the type and numbers of sugars effects the amount of antioxidant activity (Poapst et al., 1970; Hopia and Heinonen, 1999). The close relationship in the PCA2 analysis between anomeric and O-alkyl C and EDC and TEAC strongly suggests the presence of polyphenolic glycosides with antioxidant capacity in the OSB4 HA (Figures 6A,B). While the SFRC was, compared to the other HAs, on the lower side (Table 6), OSB4 HA did rank among the highest in terms of EDC and EAC (Table 6).

Two other parameters that had strong correlations to TRL-F, EAC/EDC, and SFRC were the FI and hydrophobicity (HB) indices. The FI is based on the ratio of emission intensities at 470 nm/520 nm, which characterizes the slope of the emission curve at an excitation of 370 nm (Cory and McKnight, 2005). Using parallel factor analysis (PARAFAC) on a collection of FAs, Cory and McKnight (2005) identified two “quinone-like” components, SQ1 and SQ2 that explained 84% of the variation in the FI. The excitation and emission peaks of the SQ1 component are characteristic of plant-based origins and consistent with a ground-state association between an electron donor (D, e.g., hydroxyquinone) and an electron acceptor (A, e.g., quinone)

to form a D-A charge-transfer complex (Del Vecchio and Blough, 2004; Cory and McKnight, 2005). Therefore, the fact that quinone/hydroquinone associations are largely responsible for the FI, explains the close association of FI with EAC, EAC/EDC, SFRC, and TRL-F found in this study (Figure 6). A highly significant Pearson correlation between both FI and root area (i.e.,  $0.98, p \leq 0.01$ ) was also reported by Canellas et al. (2008). Interestingly, they also reported strong correlations between both FI ( $0.89, p \leq 0.01$ ) and SFRC ( $0.78, p \leq 0.10$ ) and stimulation of  $\text{H}^+$ -ATPase activity (Canellas et al., 2008). Stimulation of  $\text{H}^+$ -ATPase activity is considered to be an indicator of HA biostimulant activity (Zandonadi et al., 2016).

The HB is calculated as the hydrophobic C/hydrophilic C ratio (Piccolo, 2002), and it has been associated with lateral root emergence (Canellas et al., 2012) and general promotion of root growth and  $\text{H}^+$ -ATPase activity in particular (Dobbss et al., 2010). The argument proposed is that low molecular weight hydrophilic molecules that are protected by hydrophobic domains are responsible for induction of lateral root growth and stimulation of  $\text{H}^+$ -ATPase activity, once they are released to the soil solution due to HA molecular conformational changes (Canellas et al., 2011). Interestingly, the presence of high concentrations of low molecular weight (LMW), diffusible, redox-active components with high quinone contents have been reported from purified peat, soil, and leonardite HAs (Yang et al., 2016; Xu et al., 2020). These components were isolated from bulk HA solutions using 3,500 and 14,000 Da molecular weight cut-off membranes and confirmed as quinonoid in nature using fluorescence spectroscopy. For the leonardite HA, EAC of the bulk, 3,500-LMWF, and the 14,000-LMWF were 1.44, 12.26, and  $28.86 \text{ meq g}^{-1} \text{ C}$ , respectively (Yang et al., 2016). Thus, the LMW diffusible plant-active components promoted by Canellas et al. (2009, 2010) are likely to contain high quantities of redox-active, quinonoid-type molecules.

In a review of research on “physiologically active substances” (PAS) that were known, through extensive studies with various plant species, to both promote and inhibit plant growth based on the chemical constitution and concentration, Flaig and co-workers (Flaig and Schmid, 1962; Flaig and Scühtig, 1962; Flaig, 1971) proposed a theory based on the abilities of these compounds to uncouple oxidative phosphorylation (OXPHOS). The PAS included lignin decomposition products e.g., *p*-hydroxybenzoic acid, protocatechuic acid, vanillic acid, vanillin, and ferulic acids; quinones, e.g., *p*-benzoquinone, toluquinone, *o*-, *m*-, *p*-xyloquinone, duroquinone, and thymoquinone; “growth substances” now referred to as plant hormones, e.g., indole-3-acetic acid (IAA), indole-3-butyric acid, naphyl-1-acetic acid, 2,4-dichlorophenoxyacetic acid (2,4-D), gibberellic acid; phenols, e.g., thymohydroquinone, *o*-hydroxyquinone, 2,4-dinitro-phenol (2,4 DNP), and 3,5-dinitro-*o*-cresol; and HS, e.g., FA and HA from different sources and produced using different isolation methods (Flaig and Scühtig, 1962). The theory proposed that with increased inorganic phosphate ( $\text{P}_i$ ) in the cell as a result of the uncoupling of OXPHOS, all reactions involving phosphorylation would be accelerated. Based on the PAS concentration, a weak uncoupling would leave enough adenosine triphosphate (ATP) present

to support cellular functions, like production of cellulose, starch, and proteins leading to increases in plant biomass accumulations. A plot of relative P/O quotients of the PAS against the negative logarithm of PAS concentration revealed a relationship between uncoupling of OXPHOS and concentration based on the chemical nature of the PAS (Flaig, 1971). The relative ability of the various PAS to uncouple OXPHOS was found to be ranked in the order of phenol carboxylic acids < plant hormones < hydroquinones/quinones < nitro phenols with concentrations ranging from  $10^{-3}$  to  $10^{-5}$  M for phenol carboxylic acids to ranging from  $10^{-4}$  to  $10^{-9}$  M for nitro phenols. This same order and dependence on concentration was also found to hold for the ability of the different PAS to promote dry matter yield of seedlings, at the concentrations where a weak uncoupling of OXPHOS occurred (Flaig, 1971).

The uncoupling of OXPHOS by these PAS is based on their ability to interfere with the coupling of mitochondrial electron transport and phosphorylation reactions, thus inhibiting ATP synthesis (Terada, 1990). OXPHOS relies on the electrochemical potential gradient ( $\Psi_{\text{mito}}$ ) that is established by the  $\text{H}^+$ -impermeable mitochondrial membrane to drive ADP phosphorylation. Some of the uncouplers, like 2,4 DNP, work via their protonophoric activity, which allows them to transport protons across the  $\text{H}^+$ -impermeable mitochondrial inner membrane and thus depolymerize the membrane (Kadenbach, 2003). In a different manner, quinones, for example, menadione (2-methyl-1,4-naphthoquinone), can undergo a one-electron reduction to the semiquinone radical by mitochondrial NADH-ubiquinone oxidoreductase activity (Powis et al., 1981). This reduction stimulates outward transmembrane electron flow across the inner mitochondrial membrane, resulting in membrane depolarization and a decrease in the ability of the mitochondria to accumulate and retain  $\text{Ca}^{2+}$  (Henry et al., 1995). A secondary, but just as deleterious effect, is that the semiquinone radicals can autoxidize at the expense of reducing molecular oxygen to the superoxide anion radical (Powis et al., 1981), which can lead further to the production of other ROS, including  $\text{H}_2\text{O}_2$  and the extremely damaging hydroxyl radical (Henry et al., 1995).

Physiologically active substances including quinones, for example, juglone (Rudnicka et al., 2014), plant hormones like IAA (Cleland, 1987; Goring et al., 1979; Felle et al., 1986; Polevoi et al., 1996; Keller and Van Volkenburgh, 1998), nitrophenols, e.g., 2,4-DNP (Homble, 1987), and HAs (Steinberg et al., 2006) also have the ability to depolymerize the plant plasma membrane (PPM)  $\Psi_{\text{pm}}$  in a similar manner to their depolarization of the inner mitochondrial membrane. Thus, quinones and semiquinone free radicals present in HAs could be apoplastically reduced, for example, by a PPM NAD(P)H oxidase (NOX), resulting in the initiation of transmembrane electron flow from cytoplasm to apoplast. There would also be a concomitant production of superoxide from reduction of molecular oxygen by the semiquinone radical or hydroquinone that are produced from reduction of the quinone or semiquinone radical, respectively. Evidence for initiation of transmembrane electron flow and superoxide radical production was produced using right side out soybean vesicles, where superoxide production was found to

be enhanced in the presence of several naphthoquinones (NQ), including menadione, juglone, 2,3-dichloro-1,4 NQ, and 1,4-NQ, by PM-bound NAD(P)H-dependent oxidases (Van Gestelen et al., 1998). The transfer of negative electrical charges (i.e., electrons) from cytoplasm to apoplast decreases the electrical contribution of the electrochemical potential gradient across the membrane, resulting in PPM depolarization.

Plant roots possess PM  $\text{Ca}^{2+}$  channels that are activated by depolarization and referred to as depolarization-activated calcium channels (DACCs) (Thion et al., 1998). As has been shown for HA PM depolarization (Steinberg et al., 2006), the extent of depolarization is elicitor concentration dependent, with higher concentrations causing greater depolarizations. Upon PM depolarization, the DACCs are activated and allow  $\text{Ca}^{2+}$  to flow into the cytosol from the apoplastic fluid or from intracellular organelles, including vacuoles and endoplasmic reticulum (Feno et al., 2019), causing a transient elevation of the free  $[\text{Ca}^{2+}]_{\text{cyt}}$  (White, 2005). The spatiotemporal pattern of the  $\text{Ca}^{2+}$  flux creates a unique “ $\text{Ca}^{2+}$  signature” that is proportional to the extent and duration of the PM depolarization, which is in turn, sensitive to and reflects the concentration of the elicitor (Qudeimat and Frank, 2009). In the case of HS, the strong correlation between both SFRG and EAC/EDC and TRL-F strongly suggests that the elicitors in HS that stimulated fine root growth in the corn seedlings, are quinones and semiquinones radicals.

Changes in  $[\text{Ca}^{2+}]_{\text{cyt}}$  occur during the transduction of a broad range of biotic and abiotic stresses (Sanders et al., 2002). Increases in apoplast to cytoplasm  $\text{Ca}^{2+}$  fluxes, in response to exposure of plant roots to HA, have also been reported (Ramos et al., 2015). It is the  $\text{Ca}^{2+}$  signature, in part, that couples extracellular elicitors, via  $\text{Ca}^{2+}$ -binding/ $[\text{Ca}^{2+}]_{\text{cyt}}$  sensor proteins, with specific intracellular responses (Lee and Seo, 2021). These responses most likely include the extensive metabolic reprogramming that has been reported to occur in plants treated with HS (Trevisan et al., 2011). Plants also respond to biotic and abiotic stress elicitors with an apoplastic production of superoxide, due to the reduction of molecular oxygen by PM NOX that are encoded by respiratory burst oxidase homologues (Rboh) genes (Torres and Dangl, 2005; Kobayashi et al., 2006; Miller et al., 2009). NOX enzymes play key roles in the stress-stimulated over production of ROS, referred to as the “oxidative burst.” Interestingly, plant NOX are stimulated directly by  $\text{Ca}^{2+}$  (Sagi and Fluhr, 2001) and increases in  $[\text{Ca}^{2+}]_{\text{cyt}}$  have been observed prior to NOX activation in response to elicitor-induced defense responses (Nurnberger and Scheel, 2001; Zhao et al., 2005). However, plants have a relatively high basal NOX activity (Doke and Ohashi, 1988; Ogawa et al., 1997; Able et al., 1998). As mentioned previously, quinones can undergo a one-electron oxidation by NOX to the semiquinone radical, which can then reduce molecular oxygen to the superoxide radical (Van Gestelen et al., 1998). Quinone reduction by NOX also stimulates transmembrane PM electron flow, which would result in PM depolarization, activation of DACCs, and increase in  $[\text{Ca}^{2+}]_{\text{cyt}}$ . The increase in free cytoplasmic  $\text{Ca}^{2+}$  could then stimulate NOX to result in greater depolymerization and ROS production. Evidence for

stimulation of trans-PM electron transport was obtained using the membrane impermeable, extracellular electron acceptor, hexacyanoferrate (HCF III). After application, reduction of HCF III to HCF II, PM depolymerization and apoplast acidification were observed (Doring et al., 1990). The reduction was attributed to trans-PPM electron transport with NAD(P)H + H<sup>+</sup> (Kruger and Bottger, 1988) or NADH + H<sup>+</sup> (Lin, 1984; Marre' et al., 1988) as the cytoplasmic electron donor. The extracellular acidification was attributed to cytoplasmic acidification and subsequent stimulation of H<sup>+</sup>-ATPase activity (Rubinstein and Stern, 1986; Marre' et al., 1988).

## CONCLUSION

A SAR study was conducted on corn seedlings using seven ore-derived, purified HAs that were subjected to extensive chemical characterization, to identify HA chemistry that drives the PBR. The ratio of pro-oxidant activities and antioxidant activities of the HAs as manifested in the EAC/EDC ratio was found to be the primary driver not only of root system morphology but also of plant biomass and shoot morphology. The HA (i.e., OSB1) with the highest EAC/EDC (*ca.* 4.1) produced corn seedlings that had the typical SIMS morphology that is characterized by smaller plants with highly ramified fine root systems. The HA (ELG) with the smallest EAC/EDC ratio (*ca.* 1.11) had the smallest impact on corn seedling growth, produced the smallest seedlings with no obvious emphasis on root or shoot growth. The largest seedlings were produced by HAs with intermediate EAC/EDC in the range of 2.0–3.5. In this range, the magnitude of the EAC and EDC resulted in plants with different morphologies. For example, a HA (i.e., OSB3) with an intermediate EAC and a lower EDC resulted in the largest plants but with highly ramified root systems. A HA (OSB4) with a high EAC and intermediate EDC resulted also in production of large plants where growth emphasis was more on the shoots. Therefore, in addition to the EAC/EDC ratio, the magnitude of the pro-oxidant activity, that is causing the stress response, is determinative.

Based on these results, we propose a mechanism of action for ore-derived HA plant biostimulation that involves the interplay of pro-oxidants, in the form of quinones and semiquinone radicals, and antioxidants, in the form of polyphenols and possibly glycones and carbohydrates. The quinones/semiquinones initiate the stress response via the stimulation of transmembrane electron flow that results in both ROS production (i.e., an oxidative burst) and membrane depolarization, the latter of which allows Ca<sup>2+</sup> flux from the apoplast into the cytoplasm. Based on the magnitude of depolarization, a specific cytoplasmic Ca<sup>2+</sup> signature is produced. As a secondary messenger Ca<sup>2+</sup>, via binding to Ca<sup>2+</sup>-sensor proteins, transmits the signature signal, resulting in specific intracellular responses that include changes to plant morphology. The greater the EAC, the greater the ROS production and extent of PM depolarization and resulting stress response. The antioxidants are able to quench the ROS and thus modulate the intensity and extent of the stress response to

greater or lesser degrees based on their concentration and radical scavenging efficiency, and thus modify the Ca<sup>2+</sup> signature.

In practical application, if the EAC/EDC ratio can be adjusted to a proportion to produce seedlings with desirable qualities, the question of which qualities result in the hardiest seedlings that provide the highest productivity, arises. For example, what would be the relative field performance of larger seedlings with more balanced root and shoot systems compared to smaller seedlings with highly ramified root systems? To a certain extent, this question could be answered by examining selected stress physiological indicators (e.g., antioxidant enzymes), photosynthetic efficiency, and other indicators of performance. However, the best indicator would be bushels of corn produced per acre, which would require a full growing season. Based on the proposed mechanism of action, the EAC/EDC ratio of a HA could be increased through quinonoid enrichment (Permanova et al., 2005) or by mixing with another HA that has a higher EAC/EDC. The EAC/EDC ratio of a HA could be reduced by mixing it with another HA with a high EDC and low EAC or possibly combining with polyphenolic materials (e.g., tannic acid). This provides a possible method, based on the proposed mode of action, for producing HAs that can be used more efficiently and effectively by the agricultural and horticultural communities.

## DATA AVAILABILITY STATEMENT

The raw data supporting the conclusions of this article will be made available by the authors, without undue reservation.

## AUTHOR CONTRIBUTIONS

RL conceived of the research, provided the purified HA, directed the bioassays, conducted the FTIR analyses, performed the PCA analyses, and wrote the manuscript. RS conducted the UV/VIS, <sup>1</sup>H-NMR, and FT ICR MS analyses and associated statistical analyses and authored the associated sections, and provided extensive manuscript editing and review. HM conducted the Molecular Modeling Model analysis and the ABTS antioxidant assay. All authors contributed to the article and approved the submitted version.

## FUNDING

The authors declare that this study received funding from Bio Huma Netics, Inc., FBSciences, Inc. R&D and HorizonAg Products. The funders were not involved in the study design, data collection, analysis, data interpretation, writing of this paper or in the decision to submit it for publication.

## ACKNOWLEDGMENTS

The authors would like to thank Dr. Michel Sander of ETH Zurich in Switzerland for the EAC and EDC determinations; Dr.

Alessandro Piccolo at CERMANU at the Università Di Napoli Federico II for the  $^{13}\text{C}$ -NMR analyses; Jennifer Spear and Tara Reed of Horizon Ag for the bioassay studies, and Horizon Ag-Products, FBSciences, Inc., R&D and Bio Huma Netics, Inc. for financial support.

## REFERENCES

- Able, A. J., Guest, D. I., and Sutherland, M. W. (1998). Use of a new tetrazolium-based assay to study the production of superoxide radicals by tobacco cell cultures challenged with avirulent zoospores of *Phytophthora parasitica* var. *nicotianae*. *Plant Physiol.* 117, 491–499.
- Aeschbacher, M., Graf, C., Schwarzenbach, R. P., and Sander, M. (2012). Antioxidant properties of humic substances. *Environ. Sci. Technol.* 46, 4916–4925.
- Aeschbacher, M., Sander, M., and Schwarzenbach, R. P. (2010). Novel electrochemical approach to assess the redox properties of humic substances. *Environ. Sci. Technol.* 44, 87–93. doi: 10.1021/es902627p
- Aeschbacher, M., Vergari, D., Schwarzenbach, R. P., and Sander, M. (2011). Electrochemical analysis of proton and electron transfer equilibria of the reducible moieties in humic acids. *Environ. Sci. Technol.* 45, 8385–8394. doi: 10.1021/es201981g
- Aguiar, N. O., Canellas, L. P., Dobbs, L. B., Zandonadi, D. B., Olivares, F. L., and Facanha, A. R. (2009). Distribuição de massa molecular de ácidos húmicos promovida do crescimento radicular. *R. Bras. Ci. Solo* 33, 1613–1623. doi: 10.1590/s0100-06832009000600010
- Aguiar, N. O., Novotny, E. H., Oliveira, A. L., Rumjanek, V. M., Olivares, F. L., and Canellas, L. P. (2013). Prediction of humic acids bioactivity using spectroscopy and multivariate analysis. *J. Geochem. Explor.* 129, 95–102. doi: 10.1016/j.gexplo.2012.10.005
- Aguirre, E., Lemenager, D., Bacalco, E., Fuentes, M., Baigorri, R., Zamarreno, A. M., et al. (2009). The root application of a purified leonardite humic acid modifies the transcriptional regulation of the main physiological root responses to Fe deficiency in Fe-sufficient cucumber plants. *Plant Physiol. Biochem.* 47, 215–223. doi: 10.1016/j.plaphy.2008.11.013
- Alewell, C. B., Ringeval, Ballabio, C., Robinson, D. A., Panagos, P., and Borrelli, P. (2020). Global phosphorus shortage will be aggravated by soil erosion. *Nat. Commun.* 11:4546. doi: 10.1038/s41467-020-18326-7
- Almendros, G., Gonzales-Fila, F. J., Martin, F., Frund, R., and Lundermann, H.-D. (1992). Solid state NMR studies of fire-induced changes in structure of humic substances. *Sci. Total Environ.* 117–118, 63–74. doi: 10.1016/j.scitotenv.2020.140063
- Baldock, J. A., Masiello, C. A., Geninas, Y., and Hedges, J. I. (2004). Cycling and composition of organic matter in terrestrial and marine ecosystems. *Mar. Chem.* 92, 39–64. doi: 10.1016/j.marchem.2004.06.016
- Bandaranayake, K. M. P., Sivakumar, V., Wang, R., and Hastings, G. (2006). Modeling the A<sub>1</sub> binding site in photosystem: I. Density functional theory for the calculation of “anion - neutral” EPR difference spectra of phyloquinone. *Vib. Spectrosc.* 42, 78–87. doi: 10.1021/bi052145u
- Bobik, K., Boutry, M., and Duby, G. (2010). Activation of the plasma membrane H<sup>+</sup> -ATPase by acid stress: antibodies as a tool to follow the phosphorylation status of the penultimate activating Thr. *Plant Signal. Behav.* 5, 681–683. doi: 10.4161/psb.5.6.11572
- Canellas, L. P., Canellas, N. O. A., Irineau, L. E. S. A., and Olivares, F. L. (2020). Plant chemical priming by humic acids. *Chem. Biol. Technol. Agric.* 7:12. doi: 10.1186/s40538-020-00178-4
- Canellas, L. P., Dantas, D., Aguiar, N. O., Peres, L. E. P., Zsogon, A., et al. (2011). Probing the hormonal activity of fractionated molecular humic components in tomato auxin mutants. *Ann. Appl. Biol.* 159, 202–211. doi: 10.1111/j.1744-7348.2011.00487.x
- Canellas, L. P., Dobbs, L. B., Oliveira, A. L., Chagas, J. G., Aguiar, N. O., Rumjanek, V. M., et al. (2012). Chemical properties of humic matter as related to induction of plant lateral roots. *Soil Sci.* 63, 315–323. doi: 10.1111/j.1365-2389.2012.01439.x
- Canellas, L. P., Facanha, A. O., Olivares, F. L., and Facanha, A. R. (2002). Humic acids isolated from earthworm compost enhance root elongation, lateral root emergence, and plasma membrane H<sup>+</sup>-ATPase activity in maize roots. *Plant Physiol.* 130, 1951–1957. doi: 10.1104/pp.007088
- Canellas, L. P., Piccolo, A., Dobbs, L. B., Spaccini, R., Olivares, F. L., Zandonadi, D. B., et al. (2010). Chemical composition and bioactivity properties of size-fractions separated from a vermicompost humic acid. *Chemosphere* 78, 457–466. doi: 10.1016/j.chemosphere.2009.10.018
- Canellas, L. P., Spaccini, R., Piccolo, A., Dobbs, L. B., Okorokova-Facanha, A. L., de Araujo Santos, G., et al. (2009). Relationship between chemical characteristics and root growth promotion of humic acids isolated from Brazilian oxisols. *Soil Sci.* 174, 611–620. doi: 10.1097/ss.0b013e3181bf1e03
- Canellas, L. P., Zandonadi, D. B., Busat, J. G., Baldotto, M. A., Imoers, M. L., Martin-Neto, L., et al. (2008). Bioactivity and chemical characteristics of humic acids from tropical soils sequence. *Soil Sci.* 173, 624–637. doi: 10.1097/ss.0b013e3181847ebf
- Chowdhury, S. (2013). Trihalomethanes in drinking water: effect of natural organic matter distribution. *Water SA* 39, 1–7.
- Cleland, R. E. (1987). “Auxin and cell elongation.” in *Plant Hormones and their Role in Plant Growth and Development*, ed. P. J. Davies (Dordrecht: Springer Netherlands), 132–148.
- Conselvan, G. B., Fuentes, D., Merchant, A., Peggion, C., Francioso, O., and Carletti, P. (2018). Effects of humic substances and indole-3-acetic acid on *Arabidopsis* sugar and amino acid metabolic profile. *Plant Soil* 426, 17–32. doi: 10.1007/s11104-018-3608-7
- Cory, R. M., and McKnight, D. M. (2005). Fluorescence spectroscopy reveals ubiquitous presence of oxidized and reduced quinones in dissolved organic matter. *Environ. Sci. Technol.* 39, 8142–8149. doi: 10.1021/es0506962
- Dai, J., and Mumper, R. J. (2010). Plant phenolics: extraction, analysis, and their antioxidant and anticancer properties. *Molecules* 15, 7313–7352. doi: 10.3390/molecules15107313
- David, J., Smejkalova, D., Hudcová, S., Zmeskal, O., von Wandruszka, R., Gregor, T., et al. (2014). The physico-chemical properties and biostimulative activities of humic substances regenerated from lignite. *Springer Plus* 2014:156. doi: 10.1186/2193-1801-3-156
- Del Vecchio, R., and Blough, N. V. (2004). On the origin of the optical properties of humic substances. *Environ. Sci. Technol.* 38, 3885–3891. doi: 10.1021/es049912h
- Devi, S., Lakher, A. K., and Kumar, V. (2019). Structural analysis and antioxidant activity of an arabinoxylan from *Malvastrum coromandelianum* L. (Garcke). *R. Soc. Chem. Adv.* 9, 24267–24279.
- Dobbs, L. B., Canellas, L. P., Olivares, F. L., Aguiar, N. O., Peres, L. E. P., Azevedo, M., et al. (2010). Bioactivity of chemically transformed humic matter from vermicompost on plant root growth. *J. Agric. Food Chem.* 58, 3681–3688. doi: 10.1021/jf904385c
- Doring, O., Luthje, S., Hilgendorf, F., and Bottger, M. (1990). Membrane Depolarization by Hexacyanoferrate (III), Hexabromoiridate (IV) and Hexachloroiridate (IV). *J. Exp. Bot.* 41, 1055–1061. doi: 10.1093/jxb/41.9.1055
- Doke, N., and Ohashi, Y. (1988). Involvement of an O<sub>2</sub> generating system in the induction of necrotic lesions on tobacco leaves infected with tobacco mosaic virus. *Physiol. Mol. Plant Pathol.* 32, 163–176.
- Falhof, J., Pedersen, J. T., Fuglsang, A. T., and Palmgren, M. (2016). Plasma membrane H<sup>+</sup>-ATPase regulation in the Center of Plant Physiology. *Mol. Plant* 9, 323–337. doi: 10.1016/j.molp.2015.11.002
- Felle, H., Brummer, B., Bertl, A., and Parish, R. W. (1986). Indole-3-acetic acid and fusicoccin cause cytosolic acidification of corn coleoptile cells. *Proc. Natl. Acad. Sci. U.S.A.* 83, 8992–8995. doi: 10.1073/pnas.83.23.8992
- Fellman, J. B., Hood, E., and Spencer, R. G. M. (2010). Fluorescence spectroscopy opens new windows into dissolved organic matter dynamics in freshwater ecosystems: a review. *Limnol. Oceanogr.* 55, 2452–2462.

## SUPPLEMENTARY MATERIAL

The Supplementary Material for this article can be found online at: <https://www.frontiersin.org/articles/10.3389/fpls.2021.758424/full#supplementary-material>

- Feno, S., Butera, G., Reane, D. V., Rizzuto, R., and Raffaello, A. (2019). Crosstalk between calcium and ROS in pathophysiological conditions. *Oxid. Med. Cell. Longev.* 2019:9324018. doi: 10.1155/2019/9324018
- Flaig, W. (1971). "Influence of metabolism of plants and its possible explanation," in *Biochemistry of Soil Organic Matter in Relation to Crop Production*, ed. W. Flaig (Braunschweig, DE, Institute of Soil Service), 192–209.
- Flaig, W., and Otto, H. (1951). Humic acids. III. Some quinones as models of the building and decomposition products of humic acids and some reduction-oxidation substances and their effect on the growth of plant roots. *Landw. Forsch.* 3, 66–89.
- Flaig, W., and Schmid, G. (1962). "Über den wirkungsmechanismus stoffwechsellaktiver substanzen," in *Eigenschaften und Wirkungen nder Gibberline, Symposium der Oberhessischen Gesellschaft für Natur- und Heilkunde. Naturwissenschaft Abt. zu Giessen*, ed. R. Knapp (Berlin: Srinter-Verlag), 25–276.
- Flaig, W., and Scühtig, H. (1962). Einfluß organischer Stoffe auf die Aufnahme anorganischer Ionen. *Agrochimica* 6, 251–264. doi: 10.1135/coccc19560251
- Garcia, A. C., Ambrosia de Souza, L. G., Pereira, M. G., Castro, R. N., Garcia-Mina, J. M., Zonta, E., et al. (2016). Structure-property-function relationship in humic substances to explain the biological activity in plants. *Sci. Rep.* 6:20798. doi: 10.1038/srep20798
- Garcia, A. C., Santos, L. A., Izquierdo, F. G., Sperandio, M., Castro, R. N., and Barbara, R. (2012). Vermicompost humic acids as an ecological pathway to protect rice plant against oxidative stress. *Ecol. Eng.* 47, 203–208. doi: 10.1016/j.ecoleng.2012.06.011
- Goring, H., Polevoy, V. V., Stahlberg, R., and Stumpe, G. (1979). Depolarization of transmembrane potential of corn and wheat coleoptiles under reduced water potential and after IAA application. *Plant Cell Physiol.* 20, 649–656.
- Grover, M., Bodhankar, S., Sharma, A., Sharma, P., Singh, J., and Nain, L. (2021). PGPR mediated alterations in root traits: way toward sustainable crop production. *Front. Sustain. Food Syst.* 4:618230. doi: 10.3389/fsufs.2020.618230
- Hatcher, P. G., Lerch, H. E. III, and Verheyen, T. V. (1990). Organic geochemical studies of the transformation of gymnospermous xylem during peatification and coalification to subbituminous coal. *Int. J. Coal Geol.* 16, 193–196. doi: 10.1016/0166-5162(90)90036-x
- Hawkes, J. A. D., Andrilli, J., Agar, J. N., Barrow, M. P., Berg, S. M., Catalán, N., et al. (2020). An international laboratory comparison of dissolved organic matter composition by high resolution mass spectrometry: Are we getting the same answer? *Limnol. Oceanogr. Methods* 18, 235–258.
- Hayes, M. H. B. (1984). "Structures of Humic Substances," in *Organic Matter and Rice*, eds S. Banta and C. V. Mendoza (Los Baños: International Rice Research Institute), 631.
- Hemida, K. A., Eloufey, A. Z. A., Seif El-Yazal, M. A., and Rady, M. M. (2017). Integrated effect of potassium humate and  $\alpha$ -tocopherol applications on soil characteristics and performance of *Phaseolus vulgaris* plants grown on a saline soil. *Arch. Agron. Soil Sci.* 63, 1556–1571. doi: 10.1080/03650340.2017.1292033
- Henry, T. R., Solem, L. E., and Wallace, K. B. (1995). Channel-specific induction of the cyclosporine a-sensitive mitochondrial permeability transition by menadione. *J. Toxicol. Environ. Health* 45, 489–504. doi: 10.1080/15287399509532011
- Hockaday, W. C., Purcell, J. M., Marshall, A. G., Baldock, J. A., and Hatcher, P. G. (2009). Electro spray and photoionization mass spectrometry for the characterization of organic matter in natural waters: a qualitative assessment. *Limnol. Oceanogr. Methods* 7, 81–95. doi: 10.4319/lom.2009.7.81
- Holdgate, G., Wallace, M., Gallagher, S. J., and Taylor, D. (2000). A review of the Traralgon Formation in the Gippsland Basin—a world class brown coal source. *Int. J. Coal Ecol.* 45, 55–84.
- Homble, F. (1987). 892-Effect of dinitrophenol on membrane potential, membrane resistance and chlorophyll fluorescence of *Chara corallina* internodal cells at various pH values. *Biochem. Bioener.* 17, 165–174. doi: 10.1016/0302-4598(87)80021-1
- Hopia, A., and Heinonen, M. (1999). Antioxidant activity of flavonol aglycones and their glycosides in methyl linoleate. *JAOCs* 76, 139–144. doi: 10.1271/bbb.65.1302
- Hou, Y., Ding, X., and Hou, W. (2015). Composition and antioxidant activity of water-soluble oligosaccharides from *Hericium erinaceus*. *Mol. Med. Rep.* 11, 3794–3799. doi: 10.3892/mmr.2014.3121
- Jannin, L., Arkoun, M., Ourry, A., Lainé, P., Goux, D., Garnica, M., et al. (2012). Microarray analysis of humic acid effects on *Brassica napus* growth: involvement of N, C and S metabolisms. *Plant Soil* 359, 297–319.
- Jimenez-Gonzalez, M., Alvarez, A. M., Carral, P., and Almendros, G. (2019). Chemometric assessment of soil organic matter storage and quality from humic infrared spectra. *Sci. Total Environ.* 685, 1160–1168. doi: 10.1016/j.scitotenv.2019.06.231
- Jindo, K., Soares, T. S., Peres, L. E. P., Lazaro, Azevedo, I. G., Aguiar, N. O., et al. (2016). Phosphorus speciation and high-affinity transporters are influenced by humic substances. *J. Plant Nutr. Soil Sci.* 179, 206–214. doi: 10.1002/jpln.201500228
- Kadenbach, B. (2003). Intrinsic and extrinsic uncoupling of oxidative phosphorylation. *Biochim. Biophys. Acta* 1604, 77–94.
- Keller, C. P., and Van Volkenburgh, E. (1998). Evidence that auxin-induced growth of tobacco leaf tissues does not involve cell wall acidification. *Plant Physiol.* 118, 557–564. doi: 10.1104/pp.118.2.557
- Kim, S., Kramer, R. W., and Hatcher, P. G. (2003). Graphical method for analysis of ultrahigh-resolution broadband mass spectra of natural organic matter, the van Krevelen diagram. *Anal. Chem.* 75, 5336–5344. doi: 10.1021/ac034415p
- Kobayashi, M., Kawakita, K., Maeshima, M., Doke, N., and Yoshioka, H. (2006). Subcellular localization of Strboh proteins and NADPH dependent O<sub>2</sub>(-)-generating activity in potato tuber tissues. *J. Exp. Bot.* 57, 1373–1379. doi: 10.1093/jxb/erj113
- Koch, B. P., and Dittmar, T. (2006). From mass to structure: an aromaticity index for high-resolution mass data of natural organic matter. *Rapid Commun. Mass Spectrom.* 20, 926–932. doi: 10.1002/rcm.2386
- Koch, B. P., and Dittmar, T. (2016). From mass to structure: an aromaticity index for high-resolution mass data of natural organic matter (Erratum). *Rapid Commun. Mass Spectrom.* 30:250.
- Kruger, S., and Botter, M. (1988). "NADH or NADPH?" in *Plasma Membrane Oxidoreductases in Control of Animal and Plant Growth*, eds F. L. Crane, D. J. Morre, and H. Low (New York, NY: Plenum Press).
- Lam, B., and Simpson, A. J. (2008). Direct <sup>1</sup>H NMR spectroscopy of dissolved organic matter in natural waters. *Analyst* 133, 263–269.
- Lamar, R. T. (2020). "Possible role for electron shuttling capacity in elicitation of PB activity of humic substances on plant growth enhancement," in *The Chemical Biology of Plant Biostimulants*, eds D. Geelan and L. Xu (Hoboken, NJ: John Wiley & Sons Ltd), 97–121. doi: 10.1002/9781119357254.ch4
- Lamar, R. T., Olk, D. C., Mayhew, L., and Bloom, R. B. (2014). A new standardized method for quantification of humic and fulvic acids in huic ores and commercial products. *J. AOAC Int.* 97, 721–730. doi: 10.5740/jaoacint.13-393
- Lambert, J. B. (1987). *Introduction to Organic Spectroscopy*. New York, NY: Macmillan.
- Lee, H.-J., and Seo, P. J. (2021). Ca<sup>2+</sup> talyzing initial responses to environmental stresses. *Trends. Plant Sci.* 26, 849–870.
- Lenssen, A., Olk, D. C., and Dinnes, D. (2019). Application of a formulated humic product can increase soybean yield. *Crop Forage Turfgrass Manag.* 5, 1–6.
- Lindroth, R. L., and Pajutee, M. S. (1987). Chemical analysis of phenolic glycosides: art, facts and artifacts. *Oecologia* 74, 144–148. doi: 10.1007/BF00377359
- Marre, M. T., Moroni, A., Albergoni, F. G., and Marre, E. (1988). Plasmalemma redox activity and H<sup>+</sup> -extrusion. *Plant Physiol.* 87, 25–29.
- McKnight, S. M., Boyer, E. W., Westerhoff, P. K., Doran, P. T., Kulbe, T., and Andersen, D. T. (2001). Spectrofluorometric characterization of dissolved organic matter for indication of precursor organic material and aromaticity. *Limnol. Oceanogr.* 46, 38–48. doi: 10.4319/lo.2001.46.1.0038
- Miller, G., Schlauch, K., Tam, R., Cortes, D., Torres, M. A., Shuliev, V., et al. (2009). The plant NADPH oxidase RBOHD mediates rapid systemic signaling in response to diverse stimuli. *Sci. Signal.* 2:ra45. doi: 10.1126/scisignal.2000448
- Milori, D. M. B. P., Martin-Neto, L., Bayer, C., Mielniczuk, J., and Bagnato, V. S. (2002). Humification degree of soil humic acids determined by fluorescence spectroscopy. *Soil Sci.* 167, 739–749. doi: 10.1097/00010694-200211000-00004
- Mingle, C. E., and Newsome, A. L. (2020). An amended potassium persulfate ABTS antioxidant assay used for medicinal plant extracts revealed variable antioxidant capacity based upon plant extraction process. *bioRxiv* [Preprint]. doi: 10.1101/2020.07.15.204065

- Moghadam, H. R. T., Mohammad, K. K., and Zahedi, H. (2014). Effect of humic acid foliar application on growth and quantity of corn in irrigation withholding at different growth stages. *Maydica* 59, 124–128.
- Monda, H., McKenna, A. M., Fountain, R., and Lamar, R. T. (2021). Bioactivity of Humic acids extracted from shale ore: molecular characterization and structure-activity relationship with tomato plant yield under nutritional stress. *Front. Plant Sci.* 12:660224. doi: 10.3389/fpls.2021.660224
- Mora, V., Bacaicoa, E., Baigorri, R., Zamarreno, A. M., and Garcia-Mina, J. M. (2014a). NO and IAA key regulators in the shoot growth promoting action of humic acid in *Cucumis sativus* L. *J. Plant Growth Regul.* 33, 430–439.
- Mora, V., Bacaicoa, E., Zamarreno, A. M., Aguirre, E., Garnica, M., Fuentes, M., et al. (2010). Action of humic acid on promotion of cucumber shoot growth involves nitrate-related changes associated with the root-to-shoot distribution of cytokinins, polyamines and mineral nutrients. *J. Plant Physiol.* 167, 633–642. doi: 10.1016/j.jplph.2009.11.018
- Mora, V., Olaetxea, M., Bacaicoa, E., Baigorri, R., Fuentes, M., Zamarreno, A. M., et al. (2014b). "Abiotic stress tolerance in plants: exploring the role of nitric oxide and humic substances," in *Nitric Oxide in Plants: Metabolism and Role in Stress Physiology*, eds M. N. Khan, M. Mobin, F. Mohammad, and F. J. Corpas (Cham: Springer International Publishing), 243–264. doi: 10.1007/978-3-319-06710-0\_15
- Muscolo, A., Cutrupi, S., and Nardi, S. (1998). IAA Detection in Humic Substances. *Soil. Biol. Biochem.* 30, 1199–1201. doi: 10.1007/s00425-010-1106-0
- Muscolo, A., Sidari, M., Logoteta, B., and Panuccio, M. R. (2010). Carboxyl and phenolic humic fractions alter the root morphology in *Arabidopsis thaliana* seedlings. *Fresenius Environ. Bull.* 19, 3146–3159.
- Muscolo, A. S., Sidari, M., Pizzeghello, D., and Nardi, S. (2009). *Effects of Humic Substances Isolated from Earthworm Faeces*. Available online at: [http://www.globalsciencebooks.info/Online/GSBOonline/images/0906/DSDP\\_3\(SI2\)/DSDP\\_3\(SI2\)45-52o.pdf](http://www.globalsciencebooks.info/Online/GSBOonline/images/0906/DSDP_3(SI2)/DSDP_3(SI2)45-52o.pdf)
- Nardi, S., Schiavon, M., and Francioso, O. (2021). Chemical structure and biological activity of humic substances define their role as plant growth promoters. *Molecules* 26:2256. doi: 10.3390/molecules26082256
- Nurnberger, T., and Scheel, D. (2001). Signal transmission in the plant immune response. *Trends Plant Sci.* 6, 372–379. doi: 10.1016/s1360-1385(01)02019-2
- Ogawa, K., Kanematsu, S., and Asada, K. (1997). Generation of superoxide anion and localization of CuZn-superoxide dismutase in the vascular tissue of spinach hypocotyls: their association with lignification. *Plant Cell Physiol.* 38, 1118–1126.
- Ohno, T., He, Z., Sleighter, R. L., Honeycutt, C. W., and Hatcher, P. G. (2010). Ultrahigh resolution mass spectrometry and indicator species analysis to identify marker components of soil- and plant biomass-derived organic matter fractions. *Environ. Sci. Technol.* 44, 8594–8600. doi: 10.1021/es101089t
- Olaetxea, M., Mora, V., Bacaicoa, E., Garnica, M., Fuentes, M., Casanova, E., et al. (2015). Abscisic acid regulation of root hydraulic conductivity and aquaporin gene expression is crucial to the plant shoot growth enhancement caused by rhizosphere humic acids. *Plant Physiol.* 169, 2587–2596. doi: 10.1104/pp.15.00596
- Onyekachi, O. G., Boniface, O. O., Gemlack, N. F., and Nichols, N. (2019). *The Effect of Climate Change on Abiotic Plant Stress: A Review*. Available online at: <https://www.intechopen.com/chapters/64791> (accessed June 12, 2021)
- Patakas, A. (2011). "Abiotic stress-induced morphological and anatomical changes in plants," in *Abiotic Stress Responses in Plants*, eds N. Tuteja and S. S. Gill (Hoboken, NJ: Wiley), 21–39. doi: 10.1007/978-1-4614-0634-1\_2
- Permanova, I. V., Kovalenk, A. N., Schmitt-Kopplin, P., Hatfield, K., Hertkorn, N., Belyaeva, E. Y., et al. (2005). Design of quinonoid-enriched humic materials with enhanced redox properties. *Environ. Sci. Technol.* 39, 8518–8524. doi: 10.1021/es050915j
- Piccolo, A. (2002). The supramolecular structure of humic substances. A novel understanding of humus chemistry and implications in soil science. *Adv. Agron.* 75, 57–134. doi: 10.1016/s0065-2113(02)75003-7
- Piccolo, A., Nardi, S., and Concheri, G. (1992a). Structural characteristics of humic substances as related to nitrate uptake and growth regulation in plant systems. *Soil Biol. Biochem.* 24, 373–380. doi: 10.1016/0038-0717(92)90197-6
- Piccolo, A., Zaccheo, P., and Genevini, P. G. (1992b). Chemical characterization of humic substances extracted from organic-waste-amended soils. *Bioresour. Technol.* 40, 272–282.
- Pizzeghello, D., Nicolini, G., and Nardi, S. (2001). Hormone-like activity of humic substances in *Fagus sylvaticae* forests. *New Phytol.* 151, 647–657. doi: 10.1046/j.0028-646x.2001.00223.x
- Poapst, P. A., Durkee, A. B., and Johnston, F. B. (1970). Root-differentiating properties of some glycosides and polyphenolic compounds found in apple and pear fruits. *J. Hort. Sci.* 45, 69–74. doi: 10.1080/00221589.1970.11514334
- Polevoi, V. V., Sinyutina, N. F., Salamatova, T. S., Inge-Vechtomo, N. I., Tankelyun, O. V., Sharova, E. I., et al. (1996). "Mechanism of auxin action: Second messengers," in *Proceedings of the International Symposium on Plant Hormone Signal Perception and Transduction*, Moscow, 223–231. doi: 10.1007/978-94-009-0131-5\_30
- Powis, G., Svingen, B. A., and Appel, P. (1981). Quinone-stimulated superoxide formation by subcellular fractions, isolated hepatocytes, and other cells. *Mol. Pharmacol.* 20, 387–394.
- Puldini, K., and Pandey, H. (2020). *Humic Acid Market Size, By Application (Agriculture, Ecological Bioremediation, Horticulture, Dietary Supplements) Industry Analysis Report, Growth Potential, Price Trends, Competitive Market Share and Forecasts, 2021 - 2-27. Report GMI1517*. (Pune: Global Market Insights), 187.
- Quaggiotti, S., Ruperti, B., Pizzeghello, D., Francioso, O., Tugnoli, V., Nardi, S. (2004). Effect of low molecular size humic substances on nitrate uptake and expression of genes involved in nitrate transport in maize (*Zea mays* L.). *J. Exp. Bot.* 55, 803–813. doi: 10.1093/jxb/erh085
- Qudeimat, E., and Frank, W. (2009). Ca<sup>2+</sup> signatures: The role of Ca<sup>2+</sup>-ATPases. *Plant Signal. Behav.* 4, 350–352.
- Ramagathan, B., Gopirama, M., Olasunkanmi, L. O., Kabanda, M. M., Yeudass, S., Bahandur, I., et al. (2015). Synthesized photo-cross-linking chalcones as novel corrosion inhibitors for mild steel in acidic medium: experimental, quantum chemical and Monte Carlo simulation studies. *RSC Adv.* 5, 76675–76688. doi: 10.1039/c5ra12097g
- Ramos, A. C., Dobbs, L. B., Santos, J. A., Fernandes, M. S., Olivares, F. L., Aguiar, N. O., et al. (2015). Humic matter elicits proton and calcium fluxes and signaling dependent on nCa<sup>2+</sup>-dependent protein kinases (CDPK) at early stages of lateral root development. *Chem. Biol. Technol. Agric.* 2:3. doi: 10.1186/s40538-014-0030-0
- Randeep, K., Ravendra, K., and Om, P. (2019). "The impact of chemical fertilizers on our environment and ecosystem," in *Research Trends in Environmental Sciences*, 69–85.
- Rani, R., Daihiya, S., Dhingra, D., Dilbaghi, N., Kim, K.-H., and Kumar, S. (2018). Improvement of the antihyperglycemic activity of nano-thymoquinone in rat model type-2 diabetes. *Chem. Biol. Interact.* 295, 119–132. doi: 10.1016/j.cbi.2018.02.006
- Re, R., Pellegrini, N., Proteggente, A., Pannala, A., Yang, M., and Rice-Evans, C. (1999). Antioxidant activity applying an improved ABTS radical cation decolorization assay. *Free Radic. Biol. Med.* 26, 1231–1237. doi: 10.1016/s0891-5849(98)00315-3
- Roomi, S., Masi, A., Conselvan, G. B., Trevisan, S., Quaggiotti, S., Pivato, M., et al. (2018). Protein profiling of *Arabidopsis* roots treated with humic substances: insights into the metabolic and interactome networks. *Front. Plant Sci.* 9:1812. doi: 10.3389/fpls.2018.01812
- Rubinstein, B., and Stern, A. I. (1986). Relationship of trans-plasmalemma redox activity of proton and solute transport by roots of *Zea mays*. *Plant Physiol.* 80, 805–811. doi: 10.1104/pp.80.4.805
- Rudnicka, M., Polak, M., and Karcz, W. (2014). Cellular responses to naphthoquinones: juglone as a case study. *Plant Growth Regul.* 72, 239–248. doi: 10.1007/s10725-013-9855-y
- Sagi, M., and Fluhr, R. (2001). Superoxide production by plant homologues of the gp91(phox) NADPH oxidase: modulation of activity by calcium and by tobacco mosaic virus infection. *Plant Physiol.* 126, 1281–1290. doi: 10.1104/pp.126.3.1281
- Sanders, D., Pelloux, J., Brownlee, C., and Harper, J. F. (2002). Calcium at the crossroads of signaling. *Plant Cell* 14(Suppl.), S401–S417.
- Schiavon, M., Pizzeghello, D., Muscolo, A., Vaccaro, S., Francioso, O., and Nardi, S. (2010). High molecular weight size humic substances enhance phenylpropanoid metabolism in maize (*Zea mays* L.). *J. Chem. Ecol.* 36, 662–669. doi: 10.1007/s10886-010-9790-6
- Scott, D. T., McKnight, D. M., Blunt-Harris, E. L., Kolesar, S. E., and Lovley, D. R. (1998). Quinone moieties act as electron acceptors in the reduction of

- humic substances by humics-reducing microorganisms. *Environ. Sci. Technol.* 32, 2984–2989. doi: 10.1021/es980272q
- Sewelam, N., Kazan, K., and Schenk, P. M. (2016). Global plant stress signaling: Reactive oxygen species at the cross-roads. *Front. Plant Sci.* 7:187. doi: 10.3389/fpls.2016.00187
- Shah, K., Kumar, R. G., Verma, S., and Dubey, R. S. (2001). Effect of cadmium on lipid peroxidation, superoxide anion generation and activities of antioxidant enzymes in growing rice seedlings. *Plant Sci.* 161, 1135–1144. doi: 10.1016/S0168-9452(01)00517-9
- Sinyayev, V. A., Toxeytova, G. A., Batorybayeva, A. A., Sasykova, L. R., Azhigulova, R. N., and Sakhipov, Y. N. (2020). A comparative investigation of the IR spectra of a carbohydrate series. *J. Chem. Technol. Metall.* 55, 724–729.
- Sleighter, R. L., Caricasole, P., Richards, K. M., Hanson, T., and Hatcher, P. G. (2015). Characterization of terrestrial dissolved organic matter fractionated by pH and polarity and their biological effects on plant growth. *Chem. Biol. Technol. Agric.* 2:9. doi: 10.1186/s40538-015-0036-2
- Sleighter, R. L., Chen, H., Wozniak, A. S., Willoughby, A. S., Caricasole, P., and Hatcher, P. G. (2012). Establishing a measure of reproducibility of ultrahigh-resolution mass spectra for complex mixtures of natural organic matter. *Anal. Chem.* 84, 9184–9191. doi: 10.1021/ac3018026
- Sleighter, R. L., McKee, G. A., Liu, Z., and Hatcher, P. G. (2008). Naturally present fatty acids as internal calibrants for Fourier transform mass spectra of dissolved organic matter. *Limnol. Oceanogr. Methods* 6, 246–253. doi: 10.4319/lom.2008.6.246
- Smith, B. C. (1999). *Infrared Spectral Interpretation: A Systematic Approach*. (Boca Raton, FL: CRC Press LLC), 265.
- Spaepen, S., and Vanderleyden, J. (2011). Auxin and plant-microbe interactions. *Cold Spring Harb. Perspect. Biol.* 3:a001438.
- Spenser, R. G., Butler, K. D., and Aiken, G. R. (2012). Dissolved organic carbon and chromophoric dissolved organic matter properties of rivers in the USA. *J. Geophys. Res. Biogeosci.* 117:G03001. doi: 10.1029/2011JG001928
- Spexard, M., Immeln, D., Thoenig, C., and Kottke, T. (2011). Infrared spectrum and absorption coefficient of the cofactor flavin in water. *Vib. Spectrosc.* 57, 282–287. doi: 10.1016/j.vibspec.2011.09.002
- Steinberg, C. E. W., Manusadan ianas, L., Grigutyte, R., Karitonas, R., Jurko-niene, S., and Pflugmacher, S. (2006). “Membrane depolarization and elevation of ROS-defensive mechanisms due to the impact of dissolved natural organic matter (NOM) in the Charophyte *Nitellopsis obtusa*,” in *Humic Substances and Soil and Water Environment*, eds L. Martin-Neto, et al. (Brazil: Embrapa, Sa o Carlos), 135–137.
- Stevenson, F. J. (1982). *Humus Chemistry*. (New York, NY: John Wiley and Sons, Inc), 443.
- Tatzber, M., Stemmer, M., Spiegel, H., Katzlberger, H., Haberhauer, C. G., Mentler, A., et al. (2007). FTIR-spectroscopic Characterization of humic acids and humic fractions obtained by advanced NaOH, Na<sub>2</sub>P<sub>2</sub>O<sub>7</sub>, and Na<sub>2</sub>CO<sub>3</sub> extraction procedures. *J. Plant Nutr. Soil Sci.* 170, 522–529. doi: 10.1002/jpln.200622082
- Terada, H. (1990). Uncouplers of oxidative phosphorylation. *Environ. Health Perspect.* 87, 213–218.
- Thion, L., Mazars, C., Nacry, P., Bouchez, D., Moreau, M., Ranjeva, R., et al. (1998). Plasma membrane depolarization-activated calcium channels, stimulated by microtubule-depolymerizing drugs in wild-type *Arabidopsis thaliana* protoplasts, display constitutively large activities and a longer half-life in ton 2 mutant cells affected in the organization of cortical microtubules. *Plant J.* 13, 603–610. doi: 10.1046/j.1365-313x.1998.00062.x
- Torres, M. A., and Dangel, J. L. (2005). Functions of the respiratory burst oxidase in biotic interactions, abiotic stress and development. *Curr. Opin. Plant Biol.* 8, 397–403. doi: 10.1016/j.pbi.2005.05.014
- Trevisan, S., Pizzeghello, D., Reperti, B., Francioso, O., Sassi, A., Palme, K., et al. (2010). Humic substances induce lateral root formation and expression of the early auxin-responsive IAA19 gene and DR5 synthetic element in *Arabidopsis*. *Plant Biol.* 12, 604–614.
- Trevisan, S., Bottom, A., Vaccaro, S., Vezzaro, A., Quaggiotti, S., and Nardi, S. (2011). Humic substances affect *Arabidopsis* physiology by altering the expression of genes involved in primary metabolism, growth and development. *Environ. Exp. Bot.* 74, 45–55. doi: 10.1016/j.envexpbot.2011.04.017
- Ueda, J., Ikota, N., Shinozuka, T., and Yamaguchi, T. (2004). Reactive oxygen species scavenging ability of a new compound derived from weathered coal. *Spectrochim. Acta Part A* 60, 2487–2492. doi: 10.1016/j.saa.2003.12.027
- Van Gestelen, P., Asard, H., Horemans, N., and Caubergs, R. J. (1998). Superoxide-producing NAD(P)H oxidases in plasma membrane vesicles from elicitor responsive bean plants. *Physiol. Plant.* 104, 653–660. doi: 10.1034/j.1399-3054.1998.1040419.x
- van Tol de Castro, T. A., Barbara, R., Tavares, O. C. H., Mello, D. F. G., Pereira, E. G., Barros, et al. (2021). Humic acids induce a eustress state via photosynthesis and nitrogen metabolism leading to a root growth improvement in rice plants. *Plant Physiol. Biochem.* 162, 171–184. doi: 10.1016/j.plaphy.2021.02.043
- Wang, J., Hu, S., Nie, S., Yu, Q., and Xie, M. (2016). Reviews of mechanisms of *in vitro* antioxidant activity of polysaccharides. *Oxid. Med. Cell. Longev.* 2016:5692852.
- Warwick, P. D. (2005). “Coal systems analysis: a new approach to the understanding of coal formation, coal quality and environmental considerations, and coal as a source rock for hydrocarbons,” in *Coal Systems Analysis*, ed. P. D. Warwick (Boulder, CO: The Geological Society of America), 12.
- Weishaar, J. L., Aiken, G. R., Bergamaschi, B. A., Fram, M. S., Fujii, R., and Mopper, K. (2003). Evaluation of specific ultraviolet absorbance as an indicator of the chemical composition and reactivity of dissolved organic carbon. *Environ. Sci. Technol.* 37, 4702–4708.
- Wershaw, R. L., Mikita, M. A., and Steelink, C. (1981). Direct carbon-<sup>13</sup>NMR evidence for carbohydrate moieties in fulvic acids. *Environ. Sci. Technol.* 15, 1461–1463.
- White, P. J. (2005). “Calcium,” in *Plant Nutritional Genomics*, eds M. R. Broadly and P. J. White (Oxford: Blackwell), 66–86.
- Xiao, Z., Hou, X., Wei, J., Ma, S., Yuan, Y., Gao, Z., et al. (2021). Relationships between structure and antioxidant capacity and activity of glycosylated flavonols. *Foods* 10:849. doi: 10.3390/foods10040849
- Xu, Z., Yang, Z., Wang, H., and Jian, J. (2020). Assessing redox properties of natural organic matters with regard to electron exchange capacity and redox active functional groups. *J. Chem.* 2020:2698213. doi: 10.1155/2020/2698213
- Yadav, S., Modi, P., Dave, A., Vijapura, A., Patel, D., and Patel, M. (2020). *Effect of Abiotic Stress on Crops*. Available online at: <https://www.intechopen.com/chapters/689945> (accessed August 11, 2021)
- Yang, Z., Kappler, A., and Jiang, J. (2016). Reducing capacities and distribution of redox-active functional groups in low molecular weight fractions of humic acids. *Environ. Sci. Technol.* 50, 12105–12113. doi: 10.1021/acs.est.6b02645
- Yohe, G. R. (1958). *Oxidation of Coal. Report of Investigations 207*. Urbana, IL: Illinois State Geological Survey.
- Zandonadi, D. B., Santos, M. P., Caixeta, L. S., Marinho, E. B., Peres, L. B. P., and Facanha, A. R. (2016). Plant proton pumps as markers of biostimulant action. *Sci. Agric.* 73, 24–28. doi: 10.1590/0103-9016-2015-0076
- Zhao, J., Davis, L. C., and Verpoorte, R. (2005). Elicitor signal transduction leading to production of plant secondary metabolites. *Biotechnol. Adv.* 23, 283–333.

**Conflict of Interest:** RL and HM were employed by Bio Huma Netics, Inc. RS was employed by FBSciences, Inc. R&D.

**Publisher’s Note:** All claims expressed in this article are solely those of the authors and do not necessarily represent those of their affiliated organizations, or those of the publisher, the editors and the reviewers. Any product that may be evaluated in this article, or claim that may be made by its manufacturer, is not guaranteed or endorsed by the publisher.

Copyright © 2021 Lamar, Monda and Sleighter. This is an open-access article distributed under the terms of the Creative Commons Attribution License (CC BY). The use, distribution or reproduction in other forums is permitted, provided the original author(s) and the copyright owner(s) are credited and that the original publication in this journal is cited, in accordance with accepted academic practice. No use, distribution or reproduction is permitted which does not comply with these terms.